JACS
JOURNAL OF THE AMERICAN CHEMICAL SOCIETY

ARTICLE

pubs.acs.org/JACS

Organic Triplet Excited States of Gold(I) Complexes with Oligo (*o*- or *m*-phenyleneethynylene) Ligands: Conjunction of Steady-State and Time-Resolved Spectroscopic Studies on Exciton Delocalization and Emission Pathways

Wei Lu,[†] Wai-Ming Kwok,[‡] Chensheng Ma,[†] Chris Tsz-Leung Chan,[‡] Ming-Xin Zhu,[†] and Chi-Ming Che*[,†]

[†]State Key Laboratory of Synthetic Chemistry, Institute of Molecular Functional Materials, and Department of Chemistry, The University of Hong Kong, Pokfulam Road, Hong Kong SAR, People's Republic of China

[‡]Department of Applied Biology and Chemical Technology, The Hong Kong Polytechnic University, Hung Hom, Kowloon, Hong Kong SAR, People's Republic of China

Supporting Information

ABSTRACT: A series of mononuclear and binuclear gold(I) complexes containing oligo(*o*- or *m*-phenyleneethynylene) (PE) ligands, namely [PhC≡C(C_6H_4-1,2-C≡C)$_{n-1}$Au(PCy_3)] (n = 2−4, **4a**−**c**), [μ-{C≡C-(1,2-C_6H_4C≡C)$_n$}{Au(PCy_3)}$_2$] (n = 1−6, 8, **5a**−**g**), [PhC≡C(C_6H_4-1,3-C≡C)$_{n-1}$Au(PCy_3)] (n = 2−4, **6a**−**c**), and [μ-{C≡C-(1,3-C_6H_4C≡C)$_n$}{Au(PCy_3)}$_2$] (n = 1, 2, **7a**,**b**), were synthesized and structurally characterized. Extensive spectroscopic measurements have been performed by applying combined methods of femtosecond transient absorption (fs-TA), fs time-resolved fluorescence (fs-TRF), and nanosecond time-resolved emission (ns-TRE) coupled with steady-state absorption and emission spectroscopy at both ambient and low (77 K) temperatures to directly probe the temporal evolution of the excited states and to determine the dynamics and spectral signatures for the involved singlet (S_1) and triplet (T_1) excited states. The results reveal that S_1 and T_1 both feature ligand-centered electronic transitions with $\pi\pi^*$ character associated with the phenyl and acetylene moieties. The $^3\pi\pi^*$ emission of the PE ligands is switched on by the attachment of [Au(PCy_3)]$^+$ fragment(s) due to the heavy-atom effect. T_1($^3\pi\pi^*$) was found to form with nearly unity efficiency through intersystem crossing (ISC) from S_1($^1\pi\pi^*$). The ISC time constants were determined to be ~50, 35, and 40 ps for **4b** and **6a**,**b**, respectively. Dual emission composed of fluorescence from S_1 and phosphorescence from T_1 were observed for most of the complexes except **5a** and **7a**, where only phosphorescence was found. The fluorescence at ambient temperature is accounted for by both the short-lived prompt fluorescence (PF) and long-lived delayed fluorescence (DF, lifetime on microsecond time scale). Explicit evidence was presented for a triplet−triplet annihilation mechanism for the generation of DF. Ligand length and substitution-dependent dynamics of T_1 are the key factors governing the dual emission character of the complexes. By extrapolation from the plot of emission energy against the PE chain length of the [Au(PCy_3)]$^+$ complexes with oligo(*o*-PE) or oligo(*m*-PE) ligands, the triplet emission energies were estimated to be ~530 and ~470 nm for poly(*o*-PE) and poly(*m*-PE), respectively. Additionally, we assign the unusual red shifts of 983 cm^{-1} from [PhC≡CAu(PCy_3)] (**1**) to [μ-{1,3-(C≡C)$_2$$C_6H_4$}{Au($PCy_3$)}$_2$] (**7a**) and 462 cm^{-1} from **7a** to [μ_3-{1,3,5-(C≡C)$_3$$C_6H_3$}{Au($PCy_3$)}$_3$] (**8**) in the phosphorescence energies to excitonic coupling interactions between the C≡CAu(PCy_3) arms in the *triplet excited states*. These complexes, together with those previously reported [Au(PCy_3)]$^+$ complexes containing oligo(*p*-PE) ligands (*J. Am. Chem. Soc.* **2002**, *124*, 14696−14706), form a collection of oligo(phenyleneethynylene) complexes exhibiting organic triplet emission in solution under ambient conditions. The remarkable feature of these complexes in exhibiting TTA prompted DF in conjunction with high formation efficiency of T_1($^3\pi\pi^*$) affords an opportunity for emission spectra to cover a wide range of wavelengths. This may have implication in the development of PE-based molecular materials for future optical applications.

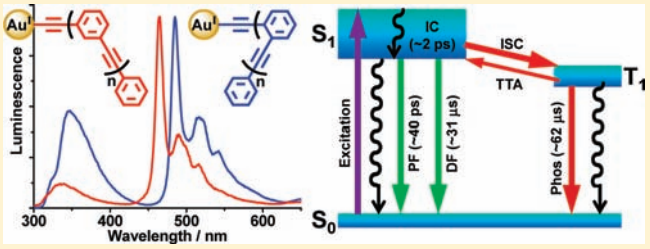

INTRODUCTION

Molecular materials based on *p*-PE(n) (PE = phenyleneethynylene, n = repeat number of the phenyleneethynylene units) have attracted much interest, due to their applications in organic optoelectronics.[1] The electron delocalization along π-conjugated backbones in these oligomers or polymers accounts for their electron conductivity, as well as their charge-transporting and photo- and electroluminescent properties. In comparison with their *p*-PE oligomeric/polymeric analogues that have a

Received: June 26, 2011
Published: August 16, 2011

linear shape and serve as molecular wires, oligo- and poly(*o*- and *m*-PE) compounds have been less studied as optoelectronic materials.[2] Recent studies with foldamers based on oligo(*o*-PE) and oligo(*m*-PE)[3] and light-harvesting dendrimers with *m*-PE components[4] have revived interest in these conjugated or cross-conjugated oligomers and polymers. While both oligo(*o*-PE) and oligo(*m*-PE) compounds are apt to form a folded or cyclic structure, only the former maintains π conjugation between two adjacent ethynylene moieties. The μ-{C≡C-1,2-C_6H_4C≡C} and μ-{C≡C-1,3-C_6H_4C≡C} fragments are rarely used as connectors or spacers for two metal centers,[5] though their 1,4-analogues μ-{C≡C-1,4-C_6H_4C≡C} have been extensively studied for this purpose.[6]

Recently, there has been a surge of interest in developing high-performance organic light-emitting devices (OLEDs) by harvesting both singlet and triplet excitons of π-conjugated oligomers and polymers,[7] This expected efficiency gain is based on the simple assumption that excitons are formed in the ratio of one singlet to three triplets upon the combination of holes and electrons in organic materials, and hence emissive triplet excitons would lead to improved efficiencies of OLEDs.[8] Numerous endeavors have been directed toward searching for practical means to achieve efficient organic phosphorescent light emitters. Several laboratories have developed protocols harnessing the heavy-atom effect on triplet excited states to "switch-on" phosphorescence from various polymer-based materials. For example, substantially enhanced intrinsic phosphorescence from poly(fluorene) was reported under ambient conditions by doping the polymer with residual palladium catalyst generated during synthesis.[9] Room-temperature, solid-state phosphorescence from some polycyclic aromatic hydrocarbons was also detected in their cocrystals with multinuclear planar mercury(II) complexes.[10] In 2010 and 2011, two research groups independently reported bright phosphorescence from pure organic crystals containing triplet-producing $^3(n-\pi^*)$ chromophores and triplet-promoting, heavy halogen-bonding atoms such as bromine.[11] More relevant, incorporation of bis(phosphine) platinum(II) moieties into the main chains of oligo- and poly(*p*-PE) has been employed to induce photo- and electroluminescence from triplet excited states of these oligomers and polymers in solutions at room temperature.[12] In general, low-energy d−d excited states of a platinum(II) ion having an unfilled d orbital can interrupt delocalization of singlet and triplet excitons along the π conjugation of *p*-PE units. This may introduce an unwanted competing nonradiative decay channel and, as a result, prohibit the observation of phosphorescence from platinum(II)-containing polymers in fluid solutions.

We previously reported an approach[13] involving the attachment of a $[Au(PCy_3)]^+$ moiety to the termini of oligo(*p*-PE) compounds through Au−C≡C ligation. The $[Au(PCy_3)]^+$ moiety can promote spin−orbit coupling, thus facilitating singlet (S_1) → triplet (T_1) intersystem crossing (ISC) while maintaining the structural integration of the π-conjugated scaffold. For this purpose, gold(I) is an sagacious choice, because its d^{10} closed-shell configuration does not allow for low-lying d−d excited states. Indeed, phosphorescence and/or delayed fluorescence (DF) from oligoynes and oligo(*p*-PE) gold(I) complexes (Chart 1) have been observed both in fluid solutions and in the solid state at room temperature.[13c,e]

As part of our continuing efforts to construct and optimize the spectral properties of PE-based molecular materials, we extended our synthetic and spectral study to meta and ortho analogues of

Chart 1. Chemical Structures of the Previously Reported Oligo(*p*-PE) Gold(I) Complexes[13c]

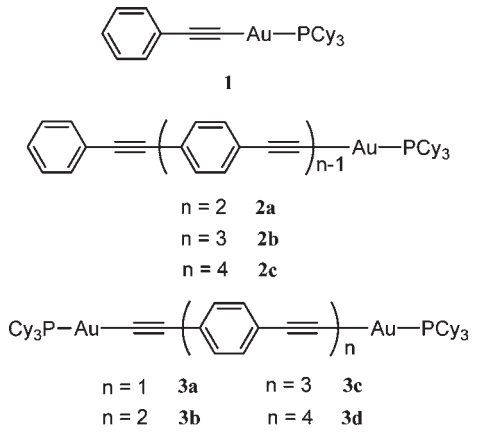

oligo(*p*-PE) gold(I) complexes.[13c] A salient feature revealed by these complexes is that most of the *o*- and *m*-PE gold(I) complexes exhibit dual emissions composed of lower energy phosphorescence and higher energy fluorescence, indicating significant engagement of both the singlet and triplet parentages in their excited states. Such a behavior contrasts sharply with that of many related complexes, such as the diimine complexes of Ru(II),[14] Re(I),[15] Pt(II),[16] and Fe(II)[17] and some cyclometalated Ir(III) complexes.[18] As reported in the literature, all of these complexes show emissions mainly from long-lived triplet excited states due to the presence of ultrafast intersystem crossing (ISC, rate of $\sim 10^{12}$ s^{-1}) that leads to extremely short singlet excited state lifetimes (tens of femtoseconds to several picoseconds) and thus a minimal involvement of fluorescence in their luminescence spectra. The Au(I) complexes described in the present study also differ from two recently reported Rh(I)[19] and Au(I)[13d] complexes containing ethynylethene ligands, which emit exclusively fluorescence (0.2−0.7 quantum yield) from relatively long lived singlet excited states (~1−3 ns lifetime), challenging the traditional picture of the heavy-metal effect on ISC. The distinct spectral features of the newly synthesized oligo(*o*-PE) and oligo(*m*-PE) gold(I) complexes herein render them attractive model systems for tackling several basic but so far unanswered issues about the excited states of light-emitting organometallic complexes. These include the spectral and energy character of the singlet and triplet excited states, the time scale and controlling factors for the ISC, and more specifically, the precise origination of the fluorescence and the interplay between the singlet and triplet states in explaining the dual emissions displayed by the complexes. Not only is the knowledge of these aspects crucial for improving the design of PE-based optoelectronic materials[1,20,21] but also the information thereof has important implications in the development of related transition-metal complexes that hold promise for many other applications such as photocatalysis, photosynthesis, and materials for photosensing and photoimaging.

We herein report the synthesis and structural characterization of series of oligo(*o*-PE) and oligo(*m*-PE) gold(I) complexes. To elucidate the excited states and help addressing the aforementioned issues, we also report detailed spectral and dynamic characterizations of several selected complexes attained by using a combination of several time-resolved methods (fs-TA, fs-TRF, and ns-TRE) and steady-state spectroscopy. By directly

monitoring the temporal evolution of excited-state spectra over a wide range of time scale, we are able to map out the excited-state relaxation cascade and to determine time constants for the ISC and lifetimes for the singlet as well as the triplet excited states. A conjunction of the steady-state and ultrafast time-resolved spectroscopic measurements also provides explicit evidence for evaluating the formation mechanism of DF and resolving the origin of the fluorescence component of the dual emissions displayed by the complexes. In addition, on the basis of the emission energy reflected by the triplet state spectra and by extrapolation of the energy from a series of oligo(*m*- *or o*-PE) gold(I) complexes to a polymer with an infinite chain length, we could estimate the triplet energy of polymeric organic materials and to discuss the effect of electron delocalization on the energy of triplet excited states with either π-conjugation (such as *o*-PE) or cross-conjugation (such as *m*-PE) character. We also reported the property of excited-state redox potentials for a selected complex.

RESULTS

Synthesis and Characterization. Four series of gold(I) complexes (Chart 2), namely $[PhC{\equiv}C(C_6H_4\text{-}1,2\text{-}C{\equiv}C)_{n-1}Au(PCy_3)]$ (n = 2−4, **4a**−**c**), $[\mu\text{-}\{C{\equiv}C\text{-}(1,2\text{-}C_6H_4C{\equiv}C)_n\}\{Au(PCy_3)\}_2]$ (n = 1−6, 8, **5a**−**g**), $[PhC{\equiv}C(C_6H_4\text{-}1,3\text{-}C{\equiv}C)_{n-1}Au(PCy_3)]$ (n = 2−4, **6a**−**c**), and $[\mu\text{-}\{C{\equiv}C\text{-}(1,3\text{-}C_6H_4C{\equiv}C)_n\}\{Au(PCy_3)\}_2]$ (n = 1, 2, **7a**,**b**), were synthesized. These complexes are higher homologues of $[PhC{\equiv}CAu(PCy_3)]$ (**1**) and analogues of $[PhC{\equiv}C(C_6H_4\text{-}1,4\text{-}C{\equiv}C)_{n-1}Au(PCy_3)]$ (n = 2−4, **2a**−**c**) and $[\mu\text{-}\{C{\equiv}C\text{-}(1,4\text{-}C_6H_4C{\equiv}C)_n\}\{Au(PCy_3)\}_2]$ (n = 1−4, **3a**−**d**);[13c] hence, they constitute a family of oligo(PE) compounds with $[Au(PCy_3)]^+$ termini. Furthermore, complexes **1**, **7a**, and $[\mu_3\text{-}\{1,3,5\text{-}(C{\equiv}C)_3C_6H_3\}\{Au(PCy_3)\}_3]$ (**8**)[13d] form a series of complexes in which the number of ethynyl groups at the benzene ring increases (from one to two and three) while maintaining meta conjugation. Studies on these complexes provide information on the effect of meta conjugation (or cross-conjugation) on electron delocalization of triplet π−π^* excited states, especially considering that the cross-conjugated organic scaffolds in these three gold(I) complexes have been investigated as modules for *m*-PE-based light-harvesting dendrimers.[22]

We adopted a deprotection/coupling and iterative-divergent approach to extend the phenylethynyl ligand to its higher homologues.[23] Thus, a Sonogashira-type iodobenzene−acetylide coupling was performed with the pivotal compounds 2-I-$C_6H_5C{\equiv}CSiMe_3$ and 3-I-$C_6H_5C{\equiv}CSiMe_3$. These two compounds were prepared from a Sonogashira coupling of (trimethylsilyl)acetylene with 2-iodoaniline and 3-iodoaniline, respectively, followed by a subsequent ^{t}BuONO/BF_3-mediated Sandmeyer reaction.[23] All of the new complexes were obtained by the reaction of $[(Cy_3P)AuCl]$ with trimethylsilyl-protected oligo(PE) ligands in a CH_2Cl_2/MeOH mixture and in the presence of NaOMe.[13] The resultant gold(I) complexes are air stable and soluble in common organic solvents, such as dichloromethane, chloroform, tetrahydrofuran, acetone, and dimethyl sulfoxide, whereas their 1,4-analogues are sparingly soluble in these solvents. The $C_\beta{\equiv}C_\alpha$−Au ligations in these complexes were confirmed by ^{13}C NMR spectroscopy. The carbon nucleus (C_α) coordinated to the Au atom appears as a doublet signal at 140 ± 5 ppm with a $^2J_{PC}$ value of ∼130 Hz, and the C_β nucleus appears as a doublet at 102 ± 2 ppm with a $^3J_{PC}$ value of ∼25 Hz,

Chart 2. Chemical Structures of Oligo(*o*-PE) and Oligo(*m*-PE) Gold(I) Complexes

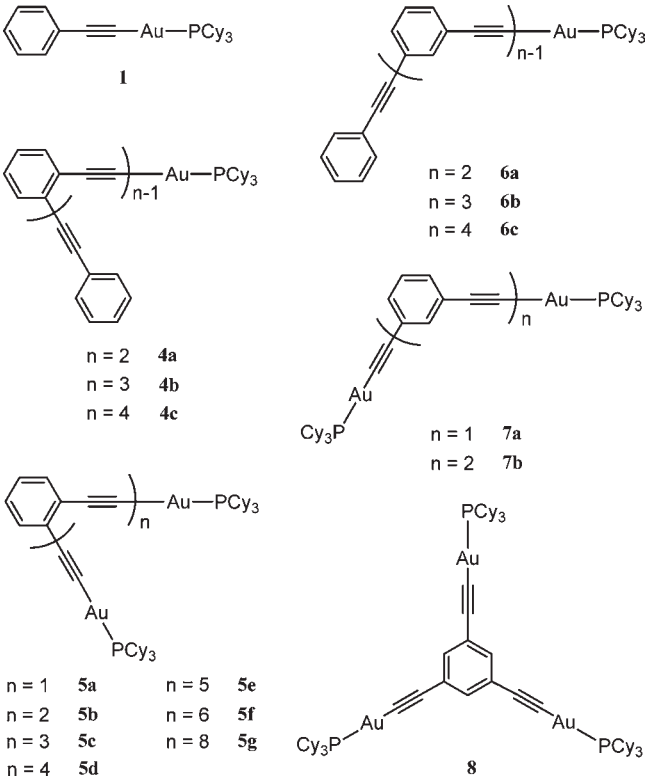

both of which are in agreement with the corresponding values for complexes **1**, **2a**−**c**, and **3a**−**d**.[13c] Other details of synthesis and NMR characterization are given in the Supporting Information.

The structure of **5d** was also determined by single-crystal X-ray crystallography. A perspective view of **5d** is depicted in Figure 1. The crystallographic data collection parameters and selected bond distances and angles are given in the Supporting Information. The bond lengths of Au−P (2.28−2.32 Å), Au−C (1.85−2.03 Å), and C≡C (1.18−1.29 Å), as well as bond angles of P−Au−C (174.3−177.5°), Au−C≡C (170.6−177.3°), and C−C≡C (173.9−179.3°), in the crystal structure of **5d** are comparable to those observed for **1**, **2a**−**c**, **3a**−**d**, and the related gold(I) σ-alkynyl complexes with phosphine ligands reported in the literature.[24] There are no short Au(I)···Au(I) contacts (<3.5 Å) in the crystal structures of these complexes. The *o*-PE(4) ligand in **5d** (Figure 1) adopts an all-transoid zigzag conformation. There is a center of symmetry located on the central C17≡C17* bond. The middle two aryl rings (B and C) are coplanar, while the two terminal aryl rings (A and D) are twisted slightly from this plane with a torsion angle of ∼17° (the dihedral angles between every two spatially neighboring aryl rings are ∠AB = 17.2°, ∠BC = 0°, and ∠CD = 17.2°). The distance (Au1−Au1*) between the two Au atoms in this extended conformation is 17.24 Å.

Steady-State Spectral Characterization of Homologues. In this section, the steady-state absorption and emission spectroscopic data of the serial gold(I) complexes with oligo(*o*-PE) (**4a**−**c** and **5a**−**g**) or oligo(*m*-PE) ligands (**6a**−**c** and **7a**,**b**) in dichloromethane (a good solvent for all the complexes under study) at 298 K and in the solid state at 77 K are presented. Furthermore, we compare these data to those of their prototype

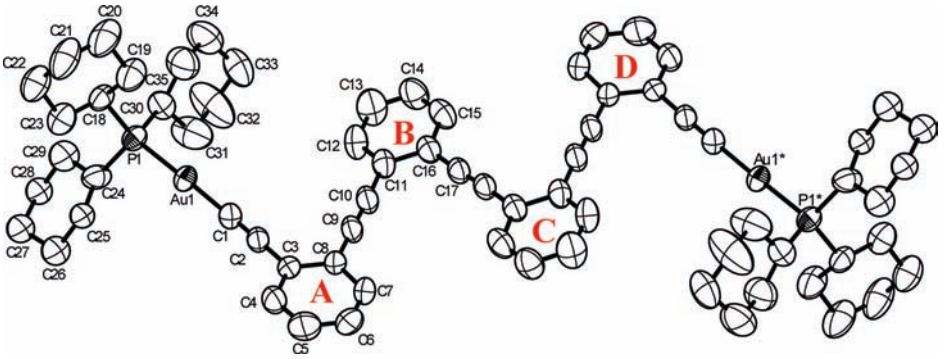

Figure 1. Perspective view of **5d** (ORTEP plot with 50% thermal probability ellipsoids, hydrogen atoms omitted for clarity). For simplicity, the aryl rings in the *o*-PE(4) ligand are labeled using block letters A−D.

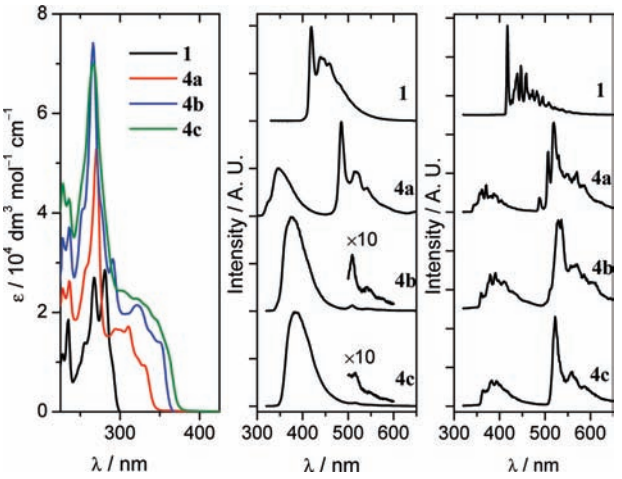

Figure 2. UV absorption (left) and normalized emission spectra of **1** and **4a**−**c** in CH_2Cl_2 at 298 K (complex concentration ~1.0×10^{-5} M) (middle) and in solid state at 77 K (right).

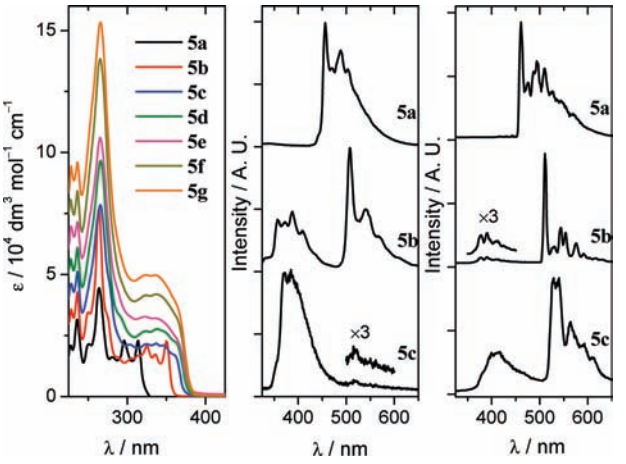

Figure 3. UV absorption spectra of **5a**−**g** (left) and normalized emission spectra of **5a**−**d** in CH_2Cl_2 at 298 K (complex concentration ~1.0×10^{-5} M) (middle) and in solid state at 77 K (right).

complex [PhC≡CAu(PCy_3)] (**1**) and their *p*-PE analogues (**2a**−**c** and **3a**−**d**).[13c] The spectra recorded for the four series of new complexes (**4a**−**c**, **5a**−**g**, **6a**−**c**, and **7a**,**b**) together with those of **1** are depicted in Figures 2−5, respectively. Emission data including the wavelength maxima and emission quantum yields are summarized in Table S1 (Supporting Information); absorption parameters in terms of peak maxima and associated extinction coefficients (ε) are given in Table S2. For help in making spectroscopic assignments, steady-state absorption and emission spectra of the corresponding free ligands were also recorded and are presented in the Supporting Information (Figures S1−S4).

In general, the gold(I) complexes with oligo(*o*-PE) or oligo(*m*-PE) ligands are emissive in fluid solutions, in 77 K glassy solutions, and in solid state. The salient features of the complexes with short PE ligands (the number of repeated PE units $n \leq 3$) are the dual emission bands found in their emission spectra recorded in degassed fluid solution at 298 K. We illustrate below the main characters revealed by the absorption and emission spectra of these complexes in solution at 298 K and in solid state at 77 K.

(1). Steady-State Absorption Spectra of Homologues in Fluid Solutions. Examination of the absorption spectra of the gold(I) *o*- and *m*-PE complexes and their comparison with that of **1** (Figures 2−5, left) and the free ligand counterparts (Figures S1−S4, Supporting Information) reveals several common features and general trends.

First, all of the complexes feature intense absorption at ~250−350 nm with molar extinction coefficients (ε) on the order of 10^4−10^5 dm^3 mol^{-1} cm^{-1}. For each series, the complexes of varying PE ligand lengths show spectra with similar profiles but progressively enhanced ε values upon lengthening the PE repeating units. For example, the maximum ε increases from ~4.4×10^4 dm^3 mol^{-1} cm^{-1} for **5a** to 15.3×10^4 dm^3 mol^{-1} cm^{-1} for **5g** and from ~4.8×10^4 dm^3 mol^{-1} cm^{-1} for **6a** to 11.3×10^4 dm^3 mol^{-1} cm^{-1} for **6c** (Figures 3 and 4 and Table S2). The increase of ε with PE ligand length appears to be more significant for the *m*-PE than for the *o*-PE series of complexes. In addition, for *o*- and dinuclear *m*-PE complexes that consist of short PE ligands, such as **4a**,**b**, **5a**−**d**, and **7a**,**b**, the lowest energy absorption bands display subtle red shifts in energy with lengthening of the PE ligand. However, such red shifts in energy are not clearly observed for the *o*-PE complexes having relatively longer PE ligands. For instance, upon a further increase of the PE unit number from **4b** ($n = 3$) to **4c** ($n = 4$) and **5d** ($n = 4$) to **5g** ($n = 8$), the absorption energy remains almost unchanged. The absorption red shift is also not observed for the mononuclear *m*-PE complexes **6a**−**c**.

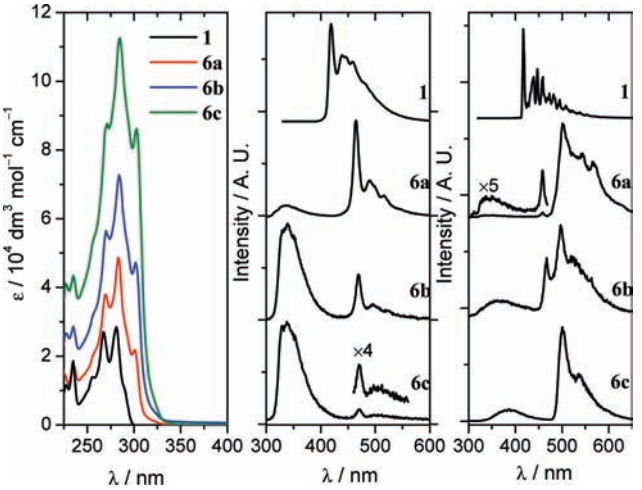

Figure 4. UV absorption (left) and normalized emission spectra of **1** and **6a**−**c** in CH_2Cl_2 at 298 K (complex concentration ∼1.0 × 10^{-5} M) (middle) and in solid state at 77 K (right).

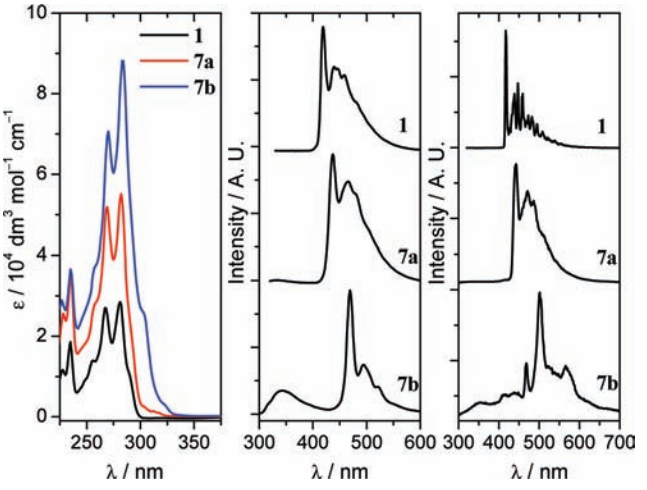

Figure 5. UV absorption (left) and normalized emission spectra of **1** and **7a**,**b** in CH_2Cl_2 at 298 K (complex concentration ∼1.0 × 10^{-5} M) (middle) and in solid state at 77 K (right).

Second, the absorption spectra of all of the complexes closely resemble those of the free ligand counterparts, with only a slight red shift in absorption energies. The extent of the red shift becomes less significant with an increase in the PE ligand length. This general similarity between the spectra of these gold(I) complexes and those of the corresponding free ligands indicates the nature of ligand-centered electronic transition(s) for the observed absorptions. The absorption bands can thus be attributed mainly to the *o*- and *m*-PE chromophores for the gold(I) oligo(*o*-/*m*-PE) complexes **4a**−**c**, **5a**−**g**, **6a**−**c** and **7a**,**b**. The subtle red shift in absorption of the gold(I) complexes from those of the corresponding free ligands parallels what we reported earlier for the oligo(*p*-PE) gold(I) analogues (**2a**−**c** and **3a**−**d**)[13c] and can be attributed to the modest stabilization of transition energy caused by the Au−C bonding interaction between the ligand and metal-containing component(s).

Another important aspect revealed by the absorption spectra is that, for each series of complexes, there are sets of absorption maxima with progressional spacings matching the vibrational frequencies of the acetylenic and phenyl groups of the PE ligands. Taking **5b** as an example, its absorption spectrum displays four peak maxima at 264, 325, 336, and 350 nm with the lowest energy band red-shifted by ∼3500 cm^{-1} from the corresponding 312 nm peak of the free ligand HC≡C(1,2-C_6H_4C≡C)$_2$H (Figure S2 in the Supporting Information). Two progressional spacings, namely 2198 and 1007 cm^{-1}, can be identified among the three maxima at 325−350 nm, and these correspond to the two kinds of characteristic vibrational stretching frequencies (acetylenic and phenyl) of the excited state of the {C≡C(1,2-C_6H_4C≡C)$_2$}$^{2-}$ moiety. For the other complexes, the absorption spectrum of **4a** (Figure 2, left) shows vibronic structures with peak maxima at 228, 236, 259 (sh), 270, 294, 310, 319 (sh), and 328 nm, corresponding to progressional spacings of 1487, 1573, 1756, and 1770 cm^{-1}; the spectra of **6a**−**c** (Figure 4, left) display absorption maxima at ∼226, 235, 260, 270, 284, and 303 nm with progressional spacings of ∼1709, 1573, 1701, and 2113 cm^{-1}; **7a**,**b** show spectra (Figure 5, left) featuring vibronic progressions very similar to those of **6a**−**c**. Obviously, all of these progressional features can be well associated with the various typical vibrational frequencies of the acetylenic and phenyl moieties of the PE ligands. Similar low-energy absorption bands with analogous vibrational progressions have been reported for [(L)AuC≡CPh] (L = PPh_3,[25] PMe_3,[26] PCy_3[13c]) and [μ-{C≡C-(1,4-C_6H_4C≡C)$_2$}{Au(PCy_3)}$_2$] (**3b**),[13c] and these absorption bands have been assigned to the ($\pi\pi^*$) transitions of the phenylacetylene ligand. On this basis, the observed absorptions can be attributed to originate predominantly from the ($\pi\pi^*$) transitions of the *o*-/*m*-PE ligands for these oligo(*o*-/*m*-PE) ligand gold(I) complexes.

Finally, on comparison with the absorption spectrum of the prototype complex **1**, the lowest energy absorption band in the spectra of **4a**−**c** (Figure 2, left) shows a gradual red shift, signaling an increase in the π conjugation of the *o*-PE with increasing PE repeating units through ortho ligation. As depicted in Figures 2 and 3 (left) and Table S2, the lowest energy absorptions of the dinuclear ortho complexes **5a**−**d** are more red-shifted from those of **1** and **4a**−**c**, suggesting further increased π conjugation as a consequence of additional [C≡CAu(PCy_3)] fragments. Apart from this, the vibronic features which appear plainly in the short PE complexes (**4a**,**b** and **5a**,**b**) become gradually less discernible with lengthening of the PE ligand and vanish eventually for the longer PE complexes (as in **4c** and **5e**−**g**). This could be attributed to an increased torsional disorder of the neighboring PE chromophoric units involved in the longer PE complexes, as reported for related platinum(II)[12b,27] complexes having *p*-PE ligands of varying lengths. Unlike those of the ortho series of complexes, the lowest energy absorption bands of mononuclear *m*-PE complexes (**6a**−**c**) closely resemble that of **1** with only a negligible red shift in energy (Figure 4, left). This is anticipated because the electron at the ground state cannot be effectively delocalized through meta conjugation. The spectra of dinuclear *m*-PE complexes **7a**,**b** show modest red shifts in energy in comparison with those of **1** and **6a**−**c** (Figure 5, left), implying an increased π conjugation induced by the extra [C≡CAu(PCy_3)] components, similar to that revealed by the absorption spectra of the *o*-PE series from **5a**−**g** to **4a**−**c**.

(2). Steady-State Emission Spectra of Homologues in Fluid Solutions. A generic feature revealed by the emission spectra of the complexes in degassed dilute CH_2Cl_2 solutions (∼1 × 10^{-5} M concentration) at 298 K (Figures 2−5, middle) is the

dual luminescence observed for all of the mononuclear *o*- and *m*-PE complexes (**4a**−**c** and **6a**−**c**) and some of the dinuclear analogues **5b**−**d** and **7b**. The spectra of these complexes show two emission bands with λ_{max} values of the high-/low-energy bands at 345−382/485−516 (**4a**−**4c**) and 337−343/465−470 nm (**6a**−**6c**) for the mononuclear complexes and at 357−377/507−523 (**5b**−**5d**) and 343/469 nm (**7b**) for those of the dinuclear complexes. Within each series (**4a**−**c**/**6a**−**c**/**5b**−**d**), when the PE unit is increased, the intensity ratio of high-/low-energy emission increases drastically (for example, from 0.5 to 17 and 28 for **4a** to **4b** and **4c**), accompanied by gradual red shifts of both emission bands. The extent of the red shift appears to be larger for the *o*-PE series **4a**−**c** (by ∼2800/1200 cm^{-1} for high-/low-energy band) and **5b**−**d** (by ∼1500/600 cm^{-1}) than for the *m*-PE complexes **6a**−**c** (by ∼500/220 cm^{-1}), consistent with the trend of red shift observed in the absorption spectra. For a given number (n) of *o*- and *m*-PE repeating units, the emission energy of the dinuclear complex (such as **5b**−**d** and **7b**) is red-shifted from that of the corresponding mononuclear counterpart (such as **4a**−**c** and **6a**), paralleling again the trend observed from the absorption spectra. On the other hand, we observed only a high-energy emission band with λ_{max} at ∼390 nm for the dinuclear complexes (**5e**−**g**), which bear relatively longer *o*-PE ligands ($n > 3$), and only a low-energy emission band with λ_{max} at 456 and 437 nm for mononuclear complexes **5a** and **7a**, respectively.

Like those of the absorption spectra (Figures 2−5, left), all of the low-energy emission bands and some of the high-energy emission bands display vibronic structures with vibronic spacings corresponding to those of PE-related vibrations. Taking the spectra of **5b** (Figures 3 and 6) as an example, the vibronically resolved high-/low-energy emission reveals two progressional spacings of 2278/2025 and 1201/1172 cm^{-1}, respectively, which correlate well with the two types of vibrational stretching frequencies (i.e., acetylenic and phenyl) of S_0 of the $\{C{\equiv}C\text{-}(1,2\text{-}C_6H_4C{\equiv}C)_2\}^{2-}$ ligand. Displayed also in Figure 6 are excitation spectra of **5a** recorded by monitoring respectively the high- and low-energy emission bands. The two excitation spectra are nearly identical, with energies and progressional spacings matching the absorption spectrum. This indicates that the high- and low-energy emissions are both derived from the same absorbing state. The low-energy bands exhibit a Stokes shift of ∼8×10^3 cm^{-1} from the lowest energy absorption band, whereas the high-energy emissions resemble the fluorescence of the related free ligands (Figures S1−S4). When these observations are taken together, the high- and/or low-energy emission can be attributed to the fluorescence and/or phosphorescence which are due to the ligand-centered radiative ($\pi\pi^*$) transition(s) from the lowest energy singlet (S_1) and triplet (T_1) to the S_0 states, respectively.

The overall emission quantum yields of these complexes are in the range of ∼0.01−0.3 (Table S1 in the Supporting Information) with the relative yield of fluorescence (Φ_{fluo}) versus phosphorescence (Φ_{phos}) varying substantially depending on the length and substitution pattern of the PE ligand. Lifetimes of both the fluorescence (τ_{fluo}) and phosphorescence (τ_{phos}) recorded in fluid solution at 298 K are on the microsecond (μs) time scale. For instance, the lifetimes τ_{fluo}/τ_{phos} of **6a** were found to be 1.6/3.2 μs and 30.5/61.5 μs in degassed dichloromethane and acetonitrile solutions, respectively. Similar dual emissions composed of remarkably long lived fluorescence and phosphorescence were reported in our previous work on gold(I)

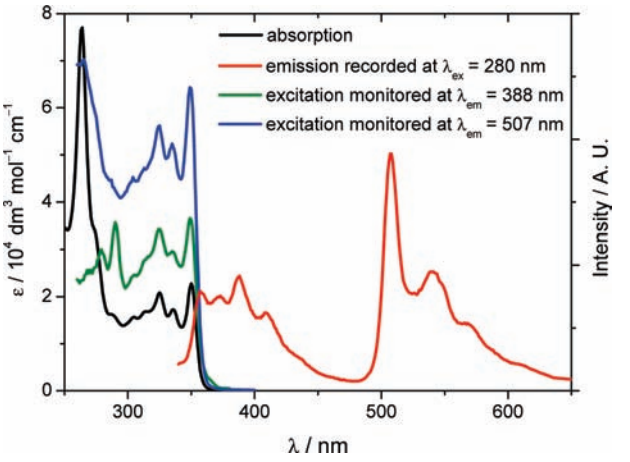

Figure 6. UV−vis absorption, excitation, and emission spectra of a CH_2Cl_2 solution of **5b** (∼1.0×10^{-5} M) at 298 K.

complexes with short *p*-PE ligands (repeating unit of PE ≤2).[13c] In that case, the fluorescence, which also features lifetimes on the order of tens of microseconds, was tentatively ascribed to DF emanating from a long-lived S_1 which was considered tentatively to originate from the T_1 via a triplet−triplet annihilation (TTA) process ($T_1 + T_1 \rightarrow S_1 + S_0$).

To explore whether TTA is relevant or not to the dual emissions exhibited by the new gold(I) *o*- and *m*-PE complexes, experiments were performed to examine the effect of the concentration of the gold(I) complex on the emission of these systems. As a typical result, steady-state emission spectra of **6a** in degassed CH_2Cl_2 solution at various concentrations were recorded (spectra shown in Figure S5 in the Supporting Information). As the complex concentration increases from 1.0×10^{-6} to 1.0×10^{-3} mol dm^{-3}, the intensity ratio (estimated using band area) of the fluorescence to phosphorescence was found to increase from ∼0.05 to ∼0.4. Thus, higher concentrations of the gold(I) complexes tend to enhance the relative involvement of fluorescence. As the energy of the absorption band changes little over this range of concentration, it follows that intermolecular process(es) occurring after the photoexcitation may play an essential role in promoting the fluorescence relative to phosphorescence. This is compatible with the TTA pathway for inducing long-lived fluorescence.

(3). Emission Spectra of Homologues in the Solid State at 77 K. As depicted in Figures 2−5 (right and middle), the emissions of all of the gold(I) complexes appear at similar wavelengths but have better resolved vibronic structures at 77 K than at room temperature (298 K) in either fluid solution or the solid state. For the complexes in each series (**4a**−**c**/**5b**−**d**/**6a**−**c**), the 77 K emissions (fluorescence and/or phosphorescence), like those at 298 K, show a gradual energy red shift upon lengthening of the PE ligand. The complexes showing dual emissions at 298 K also exhibit dual emissions at 77 K (and vice versa), but with much smaller relative contribution from fluorescence versus phosphorescence.

Considering that intermolecular processes such as TTA are anticipated to be largely inhibited in the solid state at a low temperature such as 77 K, the sizable involvement of fluorescence in the 77 K emission spectra suggests that prompt fluorescence (PF) may constitute a significant part of the high-energy emission bands of these gold(I) *o*- and *m*-PE complexes. This encourages us to probe the excited-state dynamics of these gold(I) PE complexes.

Time-Resolved Spectral Characterization of Homologues. The emission properties revealed by the steady-state measurements are determined by the dynamics of the associated emitting states, i.e. the ligand-centered $S_1(^1\pi\pi^*)$ and $T_1(^3\pi\pi^*)$, and the nature of event(s) happening during the lifetimes of these states. Thus, direct information on the dynamic evolutions and factor(s) affecting the evolution of the two states is of crucial importance in elucidating the exact origination of the dual emissions. In view of the rapid nature (tens of femtoseconds to picoseconds) of the excited-state spin crossover in the organometallic systems[14−18] on one hand and the very long emission lifetimes found for these gold(I) complexes on the other hand, to directly probe these transient states requires a time-resolved protocol that has femtosecond time resolution and at the same time covers a wide range of time scales up to microseconds. Our approach to achieve this was to combine femtosecond time-resolved spectroscopy, which coupled our broadband fs-TRF with the complementary fs-TA to directly probe early events occurring at time intervals from femtoseconds to several nanoseconds,[28] and ns-TRE spectroscopy to monitor in real time processes taking place at long time regimes of several nanoseconds and beyond. The time-resolved experiments were performed at ambient temperature with three selected complexes, the *o*-PE complex **4b** and the two *m*-PE complexes **6a**,**b**. These complexes were chosen because they bear PE ligands of different lengths (**6a** versus **6b**) or with distinct substitution patterns (**4b** versus **6b**). More importantly, they all display dual emissions but with different propensities of yielding fluorescence versus phosphorescence, typical of the trend revealed by the steady-state emission of the series of complexes (Figures 2−5). In addition, these complexes are quite soluble in acetonitrile, a relatively inert solvent for time-resolved measurements. Results obtained from the femtosecond and nanosecond spectroscopic measurements are presented in the following sections.

(1). Femtosecond Time-Resolved Characterization of Homologues. fs-TRF and fs-TA spectra obtained for **4b** and **6a**,**b** in acetonitrile solution at various time intervals after 280 nm excitation are depicted in Figures 7 and 8, respectively. The fs-TA spectra recorded at 200−6000 ps after the photoexcitation are given in Figure S6 of the Supporting Information. A common aspect revealed by temporal evolutions of the TRF and TA for all the three complexes is that the transient spectra evolve within tens to hundreds of picoseconds and persist with little change at late times from hundred of picoseconds to 6 ns (the longest delay time accessible in the present femtosecond measurements). As revealed in Figure 7, immediately after the excitation, each of the complexes shows PF (∼1 ps spectra) with location and profile resembling closely those of the corresponding steady-state fluorescence (Figures 2 and 4, middle), indicating its origination from the ligand-centered $S_1(^1\pi\pi^*)$ states of the respective systems; the spectrum then decays rapidly, achieving a remnant of the S_1 fluorescence at ∼200 ps representing in each of the cases only a minor percentage of the total fluorescence intensity.

In the fs-TA (Figure 8), the temporal evolutions for all three complexes are displayed by clear spectral transformations accompanied by sets of isosbestic points, characteristic for the occurrence of dynamic conversion from an initial precursor state to a late successor state in each of the complexes. Obviously, the TAs of **6a**,**b** are very similar, suggesting that the correlated states in the two *m*-PE complexes have analogous electronic natures and are barely affected by the inclusion of an extra PE unit in **6b** in comparison to **6a**. For both complexes, the precursor states feature broad absorptions across ∼300−800 nm (∼0.2 ps spectra) and successor states have rather sharp bands peaking at ∼430 (**6a**) or 440 nm (**6b**) (200 ps spectra); the precursor−successor spectral conversions occur with isosbestic points at ∼350 and 470 nm. The TA of **4b** differs distinctly from those of **6a**,**b** (Figure 8), reflecting different electronic configurations of the *o*- and *m*-PE complexes. For **4b**, the major spectral change is manifested by evolving from the early absorption (at ∼6 ps) featuring two λ_{max} bands at ∼440 and 620 nm to a late time spectrum (at ∼200 ps) that has a broad band at ∼400 nm along with a structured feature peaking at ∼685 nm. The temporal evolution is accompanied by isosbestic points at ∼370, 460, 675, and 700 nm. In addition, as displayed in the inset of Figure 8, before the transformation (<∼6 ps), the initial spectrum (at ∼0.4 ps) shows subtle decay concomitant with a slight blue shift of the absorption bands.

To resolve quantitatively the kinetics of the above spectral evolutions, transient fluorescence and absorption time profiles at various representative wavelengths have been examined and analyzed. Typical results obtained for the three complexes are displayed and compared in Figure 9. Corresponding data with the delay time covering up to 6 ns are given in the Supporting Information (Figure S7). The experimental time profiles ($F(t)$) were fitted by convolution of the instrument response function ($g(t)$) with an exponential function ($f(t)$) (eqs 1 and 2), where τ_i is an experimental time constant and a_i the relative amplitude associated with τ_i.

$$F(t) = \int_{-\infty}^{t} g(t')[f(t-t')]\,dt' \quad (1)$$

with

$$f(t) = \sum_{i}^{n} a_i \exp(-t/\tau_i) \quad (2)$$

Except at the very blue edge, the fluorescence time profile is nearly independent of wavelength and can be fitted by a biexponential function composed of a predominant component with time constants (denoted τ_{PF} hereafter) of ∼49, 35, and 38 ps for **4a** and **6a**,**b**, respectively, and a minor one featuring a >200 ns time constant with the relative amplitudes being 1.4%, 0.5%, and 3.6% for the respective systems. Obviously, the fast component correlates with the decay dynamics of PF from S_1 (∼380/350/360 nm profile for **4a**/**6a**/**6b**, Figure 9, left); the minor slow component (Figure S7 in the Supporting Information, left), as illustrated later, is associated essentially with the long-lived S_1 and accounts for the DF displayed by these complexes. The fluorescence at very blue edges (∼360 nm for **4b**, 325 nm for **6a**/**6b**, Figure 9, left) exhibit decay dynamics faster than those at the other wavelengths. Fitting of these profiles requires, in each of the cases, inclusion of an additional rapid component featured by a time constant of ∼1.5−2 ps, corresponding to the dynamics for collapse at the very early time of the blue edge of the transient fluorescence (Figure 7).

Kinetic analysis on the TA time profiles at various wavelengths (Figure 9, right) revealed three dynamic components for the three complexes. For each complex, depending on wavelength, this includes a major component describing decay or growth of the precursor (∼630 nm for **4b**, ∼775 nm for **6a**/**6b**) or successor state (∼400 nm for **4b**, ∼425 nm for **6a**/**6b**) and two small components, one with a rapid time constant of ∼0.1−2 ps

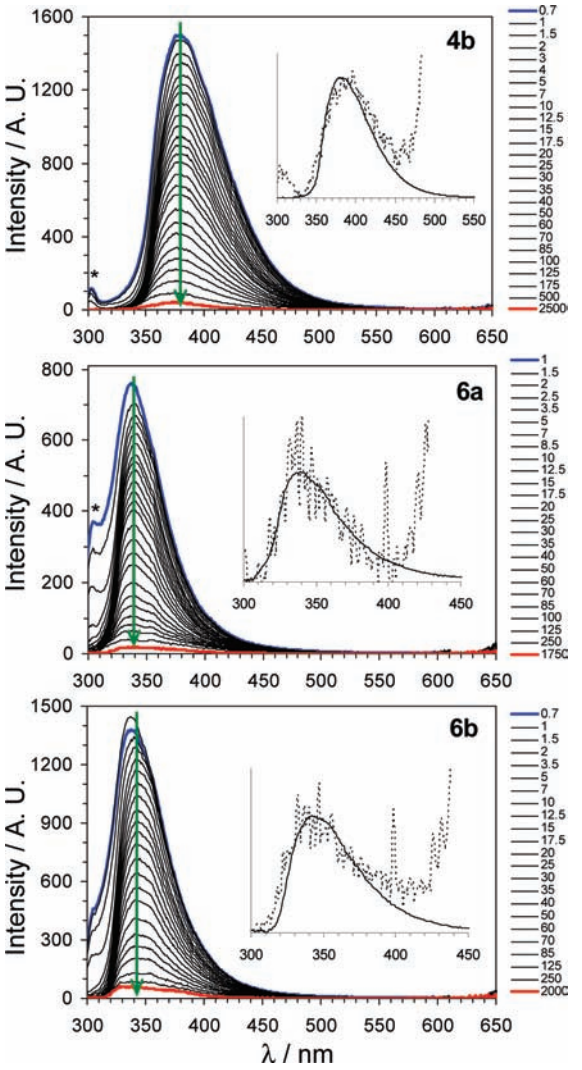

Figure 7. Femtosecond time-resolved fluorescence (fs-TRF) spectra of **4b** (top), **6a** (middle), and **6b** (bottom) in acetonitrile recorded at various indicated time delays (picoseconds) after 280 nm excitation. The insets show comparisons between fs-TRF (solid line) and ns-TRF (dotted line) recorded at 50 ps and 3 μs after the photoexcitation. The arrows indicate directions of the spectral evolutions. Asterisks denote the solvent Raman bands.

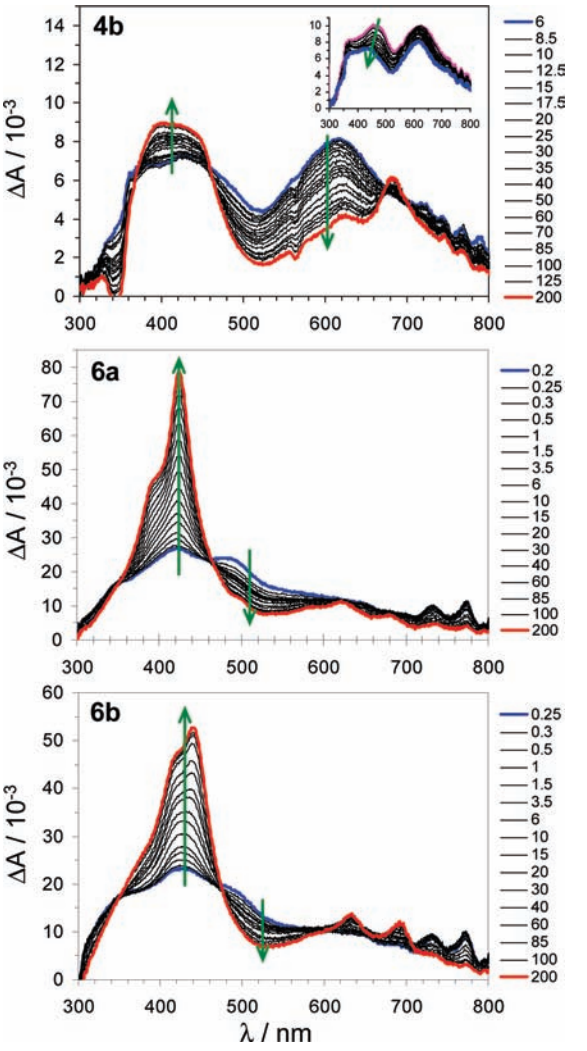

Figure 8. Femtosecond transient absorption (fs-TA) spectra of **4b** (top), **6a** (middle), and **6b** (bottom) in acetonitrile recorded at the various indicated delay times (picoseconds) after excitation at 280 nm. The inset in the top plot shows fs-TA spectra of **4b** recorded at delay times from 0.4 (pink) to 6 (blue) ps after the photoexcitation. The arrows indicate directions of the spectral evolutions.

describing the initial spectral relaxation and the other a very slow component with >200 ns time constant corresponding to persistence at long time intervals of the TA spectra (Figures S6 and S7, right). The time constants yielded for the precursor decay and correlated successor rising match with each other nicely and are ~50, 35, and 40 ps for **4b** and **6a**,**b**, respectively. Clearly, these time constants coincide exactly with the major TRF decay times (τ_{PF}) obtained for the respective systems, indicating that the correlated spectral evolutions revealed by the TRF (Figure 7) and TA spectra (Figure 8) must originate from the same excited-state processes, which can be attributed to the ISC from S_1 to T_1. Consequently, the precursor and successor states observed in the fs-TA are due to S_1 and T_1, respectively, and the associated spectra provide the absorption signatures for the two states in each of the complexes.

From the steady-state absorption (Figures 2 and 4) and electronic nature of the S_1 state, the radiative rate constant of S_1 ($k_r(S_1)$) can be estimated to be on the order of 10^8 s^{-1} for the three complexes, equivalent to radiative lifetimes of several to 10 ns in each case.[29] Given this and a minor involvement of the other nonradiative process(es), it emerges that the ISC plays a primary role in deactivating the photoprepared, brightly emissive S_1. As a result, the S_1 decay time (τ_{PF} = ~35−50 ps) can be ascribed as the ISC time for the corresponding complex. It is crucial to note at this point that the similar ISC times displayed by **4a** and **6a**,**b** suggest that the ISC rate of these gold(I) complexes is barely affected by the substitution pattern (ortho versus meta) and length (n = 2 versus n = 3) of the PE ligand system. With these ISC times, a close to unity efficiency of ISC can be derived, consistent with those reported for many other organometallic complexes.[12−18] When the measured lifetime (τ_T) and quantum yield (Φ_T) for T_1 are combined (Table S1), the k_r value for T_1 ($k_r(T_1)$) is deduced to be no greater than 10^4 s^{-1}, lower by around 4 orders of magnitude than the value of $k_r(S_1)$. This indicates a very "dark" nature of T_1 compared to S_1,

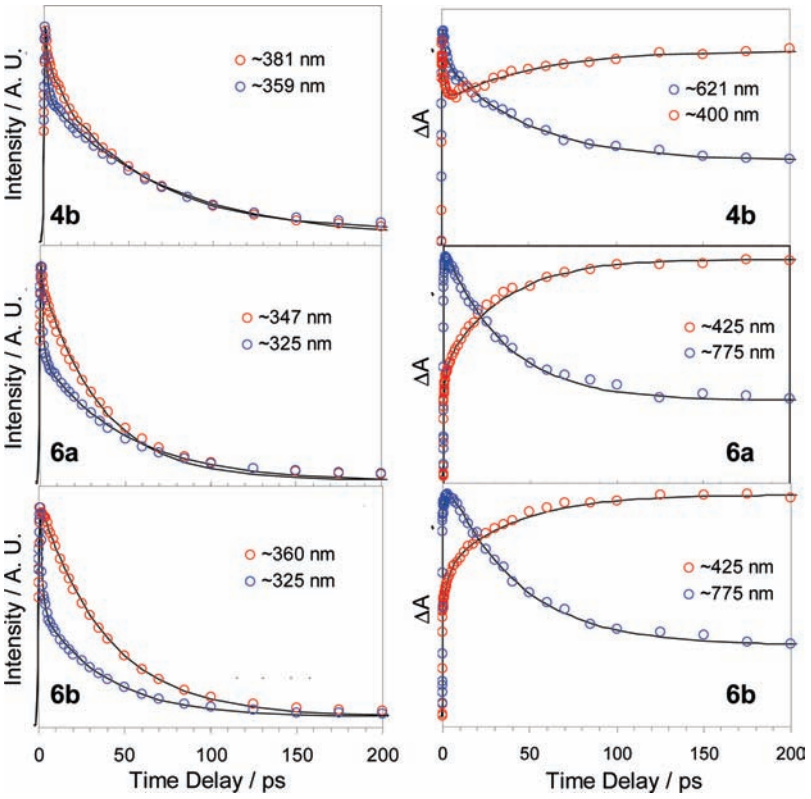

Figure 9. Normalized experimental (circles) and fitted (solid lines) kinetic time profiles at the indicated wavelengths obtained from femtosecond time-resolved fluorescence (left) and transient absorption (right) for **4b** (top), **6a** (middle), and **6b** (bottom) in acetonitrile with excitation at 280 nm.

accounting for the lack of T_1 emission in the fs-TRF spectra (Figure 7) of the three complexes.

The early ~1−2 ps dynamics, manifested by the narrowing at blue edge of the fs-TRF (Figure 7) and subtle spectral relaxation of the fs-TA (Figure 8), can be attributed to an ensemble of relaxation processes of the initial photogenerated S_1, such as vibrational cooling and conformation relaxation. According to the steady-state absorption and fluorescence (Figures 2 and 4), the 280 nm excitation may introduce $\sim(7-4) \times 10^3$ cm^{-1} excess vibrational energy above the 0−0 level of the initial S_1. A vibrationally hot excited state is known to feature a spectrum slightly broader than that from the relaxed state and may relax within several picoseconds after the excitation.[30] Previous time-resolved studies on related oligo(*p*-PE) systems without coordinated metal ions revealed similar early-time TRF and TA spectral relaxations, which were found to be relevant to intramolecular structural variation for attaining a more constrained relative PE orientation in S_1 compared to S_0.[27a,31] It is likely that analogous conformational relaxation may also apply to the gold(I) complexes, especially for the *o*-PE complex **4b**, which was found to have a greater extent of fs-TA relaxation than did **6a**,**b** (inset in Figure 8).

It is noteworthy that, with the ISC ($S_1 \rightarrow T_1$) and S_1 relaxation time determined to be ~35−50 ps and ~1−2 p,s respectively, our result ascertains that, for the gold(I) complexes investigated herein, T_1 is formed on the tens of picoseconds time scale from fully relaxed S_1. This is in contrast with most of the reported cases, where the ISC of organometallic complexes was found to occur on an ultrafast time scale (tens to hundreds of femtoseconds) from vibrationally hot S_1 prior to any relaxation processes.[12−18]

(2). Nanosecond Time-Resolved Characterization of Homologues. It follows from the femtosecond time-resolved measurements that, for all three complexes, at about several nanoseconds after the excitation, the system population is dominated by T_1 and a small percentage of the S_1 state (corresponding to the >200 ns time component observed in fs-TRF and TA). Understanding the spectral and dynamic character of these transient excited states over a long time scale (nanoseconds to milliseconds) is essential for evaluating the formation mechanism of the long-lived fluorescence and the detailed composition of the dual emission. For this purpose, ns-TRE experiments achieved by employing a time-gated detection technique have been performed for the selected complexes. By using a gating time (variable, 1 ns−1 ms) much more prolonged than that used in the fs-TRF (~1 ps), this measurement, upon appropriate setting, allows detection of the weak transient emission from both the T_1 and residual S_1 states.

Figure 10 depicts ns-TRE spectra obtained for complexes **4a** and **6a**,**b** at time delays longer than 1 μs after excitation at 280 nm. The spectra were measured at ambient temperature with deoxygenated acetonitrile solutions ($\sim10^{-5}$ M) of the respective complexes. Representative spectra obtained at delay time from tens to hundreds of nanoseconds after the excitation are given in the Supporting Information (Figure S8). For each complex, the spectra reveal dual emissions with the respective profiles (including the vibronic features) and locations (but not relative intensity) matching exactly those of the steady-state emission spectra recorded at 298 K, indicating their attribution to DF and phosphorescence, respectively. More explicitly, a direct comparison between the time-resolved spectra of the DF and PF (insets in Figure 7) reveals identical features, attesting that the two

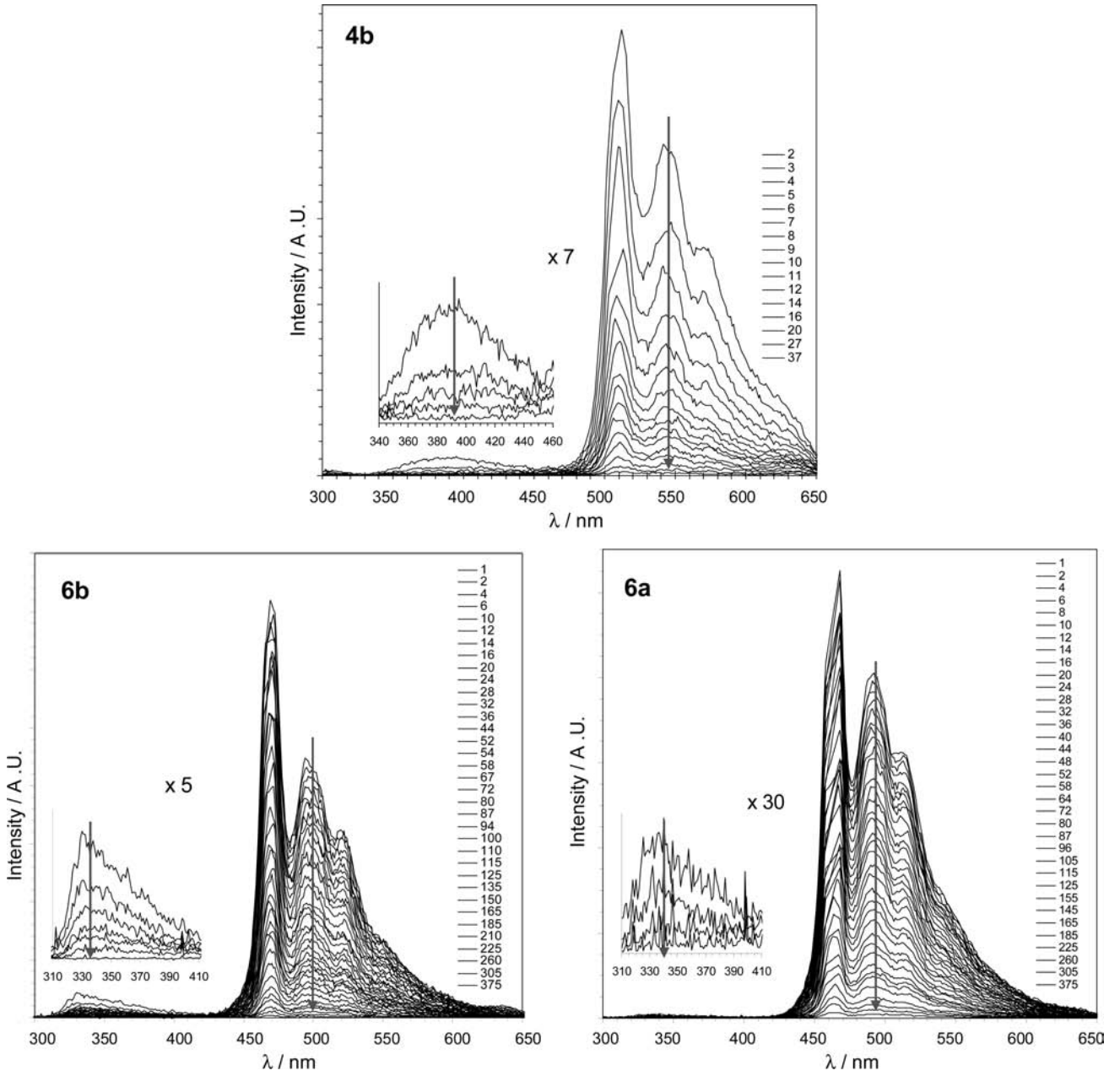

Figure 10. Time-resolved emission spectra of **4b** and **6a**,**b** recorded with 100 ns gate width at the indicated time intervals (μs) after 280 nm excitation in acetonitrile. The insets show magnified spectra corresponding to the delayed fluorescence of the respective systems. The arrows indicate directions of the spectral evolutions.

emissions, though occurring at distinctly different time regimes (10 ps/10 μs for PF/DF), have essentially the same intrinsic origin, i.e., the ligand-centered radiative $\pi\pi^*$ $S_1 \rightarrow S_0$ transition, in each of the cases. This allows exclusion of any other probable assignment (such as excimer etc.) to the long-lived fluorescence displayed by these complexes.

The spectra acquired revealed that, at early time, the emission due to fluorescence prevails over that of phosphorescence (Figure S8); however, as a result of the much faster decay of the fluorescence compared to phosphorescence, the emission at relatively later times (at >100 ns) are overwhelmingly dominated by the phosphorescence (Figure 10). Bearing in mind the much lower k_r value for T_1 ($k_r(T)$) as compared to that for S_1 ($k_r(S)$), this observation testifies to the minute involvement of S_1 relative to T_1 during the long time relaxation of the excited states. For example, according to the measured intensity ratio of transient fluorescence to phosphorescence, the population fraction of S_1 to T_1 appears to be no greater than 10^{-4} at delay times beyond tens of nanoseconds after the excitation.

Figure 11 shows the kinetic decay traces of the DF and phosphorescence obtained from the spectral data (Figure 10) for the three complexes. The decay profiles can be well fitted by a single-exponential function, yielding lifetimes for DF and phosphorescence (τ_{DF}/τ_{phos}) of 1.9/4.3 μs for **4b** and 30.5/61.5 and 32.8/63.7 μs for **6a**,**b**, respectively. Note that for each complex the τ_{DF} value is about half of τ_{phos} and that τ_{DF}/τ_{phos} for **6a** is

very similar to that of **6b** and both are substantially longer than the lifetime of **4b**. A parallel experiment performed under aerated conditions revealed simultaneous shortening of both the τ_{DF} and τ_{phos}, suggesting that involvement of oxygen may lead to synchronous quenching of both types of emissions. As an illustrative example, τ_{DF}/τ_{phos} was found to be ~0.4/0.5 μs for **6a** under the aerated conditions. Considering a typical oxygen concentration of $\sim 10^{-3}$ M in the aerated solution and assuming a $<10^{-5}$ M concentration under the deoxygenated conditions, according to the measured lifetimes, the fluorescence and phosphorescence quenching rate constants k_q can be estimated to be $\sim 2.3 \times 10^9$ and 2.0×10^9 M^{-1} s^{-1}, respectively.[29] The nearly identical quenching rate constants substantiate a strong kinetic correlation between the two emissions, indicating that both emissions should have the same dynamic origin.

The DF and thus the long-lived S_1 could be produced by two kinetic pathways: TTA ($T_1 + T_1 \rightarrow S_1 + S_0$) and a thermally activated triplet-to-singlet upconversion ($T_1 \rightarrow S_1$).[29,32,33] The thermally activated process is unimolecular in nature and the decay time of DF is expected to be identical with that of phosphorescence.[29,32,34] TTA, on the other hand, is a bimolecular process corresponding to mutual annihilation of T_1, leading to formation of the singlet excited state (S_1) of one partner.[29,32] According to its rate law, a key characteristics of TTA-induced DF is that the DF decays exponentially at long times with half the phosphorescence lifetime.[32,35,36] Thus, our results on the lifetimes (τ_{DF}/τ_{phos}) in conjunction with the concentration and oxygen quenching effects provide coherent and solid evidence for the TTA mechanism in accounting for the observed DF and long-lived S_1. It is noted that although TTA-induced DF has been considered a rather common phenomenon in various organic systems (especially conjugated polymers),[32,35,37] it has been scarcely studied for transition-metal complexes.[38] To this end, the gold(I) complexes investigated herein may provide the first firmly proven case for the involvement of such a process in transition-metal complexes, to the best of our knowledge.

Estimated Excited-State Redox Potential of 4a. The $^3(\pi\pi^*)$ states of these gold(I) arylacetylide complexes are strong photoreductants.[13c] Oxidative quenching experiments of the triplet emission of **4a** in acetonitrile by a series of pyridinium acceptors[39] were undertaken, and the results are presented in Table S3 in the Supporting Information. Nonlinear least-squares fitting of ln k_q' vs $E^o(A^+/A)$ using the Rehm−Weller model was performed (see the Supporting Information for a diagram). The excited-state redox potential of $E^o(\mathbf{4a}^+/\mathbf{4a}^*)$ and the reorganization energy (λ) were determined to be −1.84 V vs $Fc^{+/0}$ and 0.95 eV, respectively. This potential is lower than that (less than −1.70 V vs $Fc^{+/0}$) estimated from the equation $E^o(\mathbf{4a}^+/\mathbf{4a}^*) = E^o(\mathbf{4a}^+/\mathbf{4a}) - E_{0-0}$, where E_{0-0} is calculated from the spectroscopic data (2.56 eV (485 nm)) and $E^o(\mathbf{4a}^+/\mathbf{4a})$ is approximated from E_{pa} obtained in cyclic voltammetry measurements (−0.86 V vs $Fc^{+/0}$; see the Supporting Information for CV data). The zigzag *o*-PE gold(I) complex **4a** is a strong photoreductant, comparable to its linear *p*-PE gold(I) analogue **2a** ($E^o(\mathbf{2a}^+/\mathbf{2a}^*) = -1.43$ V vs $Fc^{+/0}$)[13c] in the excited state.

DISCUSSION

Deciphering the Ligand-Dependent Dual Emission. To unravel the underlying cause for the dependence of steady-state emissions on the ligand length and substitution pattern of PE ligands, it is necessary to not only resolve the emission compositions included but also and more importantly identify the major factor(s) that influence(s) dynamic interplay between the S_1 and T_1 states and thus the varying propensity for emitting fluorescence versus phosphorescence of these complexes.

Taking together the femtosecond to nanosecond and nanosecond to microsecond time-resolved data of **4a** and **6a**,**b** (Figures 7 and 11), it is clear that, except for the phosphorescence which accounts for the low-energy component of the dual emissions, both PF and DF contribute to the high-energy fluorescence component of the these complexes. Our time-resolved spectroscopic data show that dynamic coupling between the S_1 and T_1 states occurs as a consequence of two consecutive events that take place in two discrete time regimes (Scheme 1). First, the photopopulated S_1, after (vibrational and conformational, etc) relaxation, transforms into T_1 through ISC with time constants of ~35−50 ps. This process, which was found to be barely affected by the length and substitution pattern of the PE ligand, leads to a rapid quenching of the PF and a nearly unity yield of T_1. Taking the time constants (τ_{PF}) and radiative rate constants ($k_r(S_1)$), the quantum efficiency of PF can be estimated to be on the order of $\sim 10^{-2}-10^{-3}$ for the three complexes. In the second phase (nanoseconds to microseconds), T_1 undergoes intermolecular TTA, resulting in partial conversion of the T_1 population to the S_1 manifold that gives DF featured by lifetime about half of that of the phosphorescence from T_1. Owing to the very long lifetime, the DF, though derived from S_1 that carries only a minute fraction of the excited-state population, may contribute significantly to the collective fluorescence, as seen in the steady-state emission. In addition, given the respective "bright" and "dark" natures of the S_1 and T_1 states ($k_r(S_1) \gg k_r(T_1)$), the TTA-induced T_1 to S_1 population conversion, even occurring to a small extent, may cause a pronounced increase of the fluorescence at the expense of phosphorescence in the steady-state emission.

When the fluorescence decay dynamics obtained in the various time regimes are combined (Figures 9 and 11), the percentage involvement of DF (Figures 2 and 5, middle) was estimated to be ~90% in the case of **6b** and ~60% and 52% for **6a** and **4b**, respectively. However, the larger involvement of DF in **6b** compared to that of **6a** and **4b** appears to arise from different causes. For **6a**,**b**, the difference in the DF involvement is mainly due to the greater weighting factor of DF as depicted in fs-TRF (~3.6% for **6b** and ~0.5% for **6a**), which according to the rate law[35,36] is indicative of a higher efficiency of TTA in **6b** than in **6a**. Given the different PE lengths ($n = 1$ versus $n = 2$ for **6a** versus **6b**), it follows that the TTA efficiency tends to increase upon elongating the PE ligand. Taking into account the analogous quantum yield of PF, the observed larger fluorescence to phosphorescence intensity ratio in the 298 K steady-state emission of **6b** as compared to that of **6a** (Figure 4, middle) is reasonable. This rationale may also be extended to a further increase in the fluorescence/phosphorescence intensity ratio from **6b** ($n = 2$) to **6c** ($n = 3$) (Figure 4, middle) and to the very similar trend revealed in the 298 K emission spectra of the other series of complexes (**4a**−**c**/**5a**−**d**/**7a**,**b**; Figures 2, 3, and 5, middle).

In a comparison between **4b** and **6b**, in addition to a slightly lower TTA efficiency, as suggested by the fs-TRF (Figure 7 and 9, left), the much lesser DF involvement in **4b** seems to relate largely to the DF lifetime of **4b** (1.9 μs) being shorter than that of

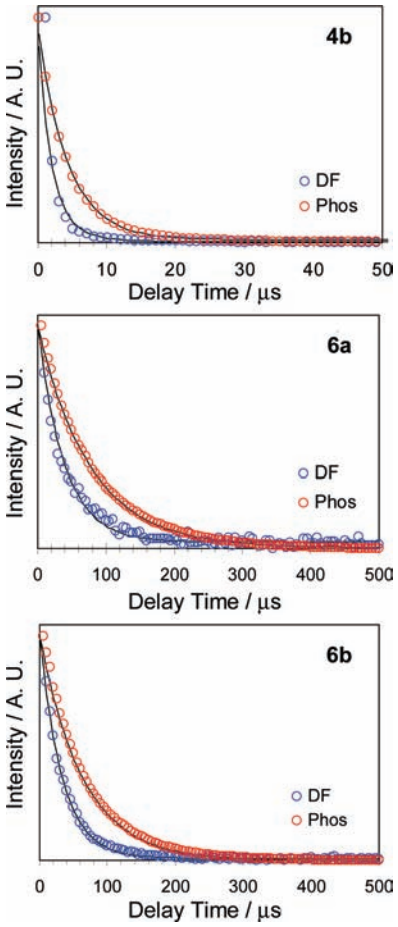

Figure 11. Normalized experimental (circles) and fitted (solid lines) phosphorescence (Phos) and delayed fluorescence (DF) kinetic traces for **4b** and **6a,b** after 280 nm excitation in acetonitrile.

6b (32.8 μs). Considering the ligand-centered $\pi\pi^*$ character of the excited states (S_1 and T_1) and the known photochemical instability of the *o*-PE systems (a possible Bergman cyclization reaction),[3a,40] the short lifetime of **4b** is most likely caused by the presence of a competing photochemical decay path associated with the *o*-PE unit of the complex. The photochemical reaction, which is accessible especially to the *o*-PE complexes, may occur mainly on the T_1 (major species in nanosecond to microsecond time regime) and compete with the TTA for quenching population of the T_1. The inclusion of this extra nonradiative decay channel for the *o*-PE rather than the *m*-PE complexes may constitute an important factor for the less effective TTA and shorter S_1/T_1 lifetimes (τ_{DF}/τ_{phos} = 1.9/4.3 μs) observed for **4b** as compared to **6b** (τ_{DF}/τ_{phos} = 32.8/63.7 μs). This also affords a rationale for the different emission behaviors of the two complexes, such as the lower emission yield of **4b** (0.09) compared to that of **6b** (0.12) (Table S1) and in particular the minimal involvement of the phosphorescence in the steady-state emission of **4b** (Figure 2, middle). In view of the similar features (diminished phosphorescence with increased repeat PE unit number) in the emission spectra (Figures 2 and 3, middle), such a substitution-specific effect may well be operative in the cases of the other *o*-PE complexes (**4a,c**), including the binuclear counterparts (**5b**−**d**).

As a corollary of the above, the following insights for the emission behavior of these *o*- and *m*-PE gold(I) complexes

Scheme 1. Dynamics and Deactivation Diagram Proposed for the Gold(I) Complexes[a]

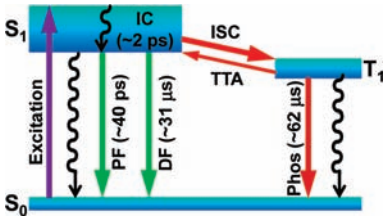

[a] The time constants denoted are from the results on **6b**. The curved lines indicate the decay paths due to nonradiative transitions.

emerge: (i) a fundamental feature, which is common to most of the complexes, is the nearly unity efficiency of ISC and the substantial involvement of PF due to the tens of picoseconds lifetimes of photogenerated S_1; (ii) the ligand-dependent T_1 efficiency in giving TTA to produce DF (favored by longer PE ligand) and the possible photochemical stability play a decisive role in regulating the actual appearance of fluorescence versus phosphorescence in the overall emission. This picture, in addition to providing a cohesive interpretation for the emissions at ambient temperature (as described above), also agrees well with and is in effect strengthened by the low-temperature (77 K) emissions (Figures 2−5, right) displayed by the series of complexes. The observation that, for most complexes (**4a**−**c**, **5b**−**d**, **6a**−**c**, and **7b**), the emission at 77 K is dominated by phosphorescence together with a sizable contribution of fluorescence corroborates nicely the rapid ISC and implies that, for those complexes in the present study that are not covered in the time-resolved measurements, their ISC may proceed at time scales comparable to those determined for **4b** and **6a,b**. In addition, the much lesser fraction of fluorescence in emission at 77 K as compared to that at 298 K substantiates and confirms the important contribution of the TTA-originated DF to the room-temperature fluorescence.

It is worthwhile to note that, although the very high ISC efficiency shown by the series of gold(I) *o*-and *m*-PE complexes demonstrates the success of our strategy in exploiting the heavy-metal effect to promote triplet formation, the ISC times revealed for the complexes are much slower than the ultrafast ISC times reported for many other metal−organic complexes.[14−18] In this respect, a notable feature revealed by the series of complexes is the lack of fluorescence emission (at 298 K and even 77 K) in the parent complex **1** and the dinuclear complexes **5a** and **7a**. This implies that ISC times for these complexes must be much faster than those (usually tens of picoseconds) for the other complexes. While this finding for **5a** and **7a** might be attributed to the inclusion of two Au atoms, the common inclusion of one Au atom in **1** as in the two series of mononuclear complexes (**4a**−**c** and **6a**−**c**) underlines the crucial role played by the detailed composition of the ligand in alternating the rate of ISC. In view of the increasing current concern about the efficiency and factor(s) affecting the efficiency of the heavy-metal effect in encouraging ISC,[13e,14−19] the ISC time constants presented here for the several gold(I)-containing complexes contribute important photophysical parameters for better assessment of this widely used but so far unclear effect.

Exciton Delocalization in *p*-PEs, *o*-PEs, and *m*-PEs. Figure 12 (left) displays the emission spectra of the three mononuclear

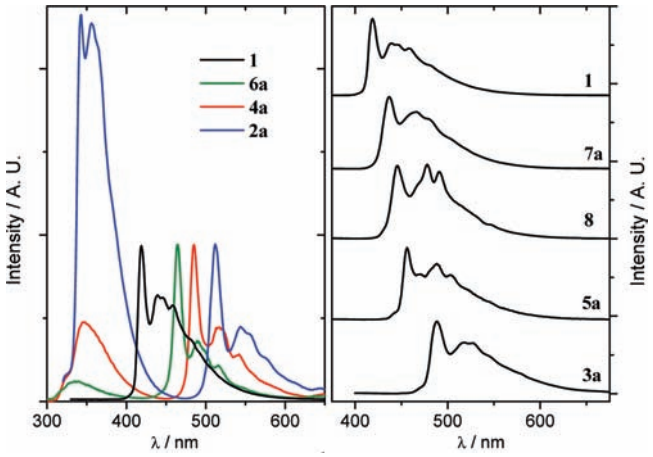

Figure 12. Emission spectra of (left) **1**, **2a**, **4a**, and **6a** and (right) **1**, **3a**, **5a**, **7a**, and **8** in CH_2Cl_2 at 298 K.

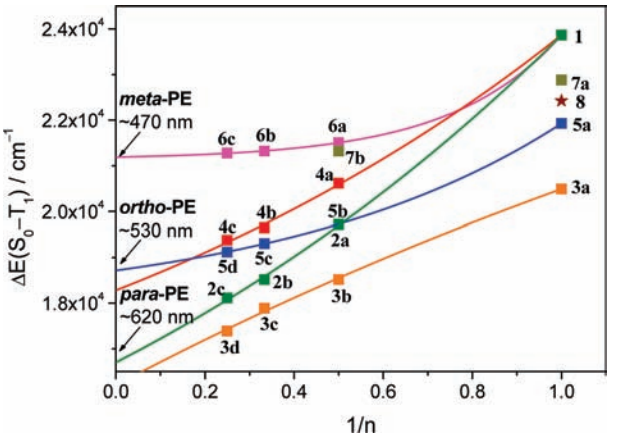

Figure 13. Plot of $\Delta E(S_0-T_1)$ against $1/n$ (n is the number of the repeating PE units in the oligo(PE) gold(I) complexes).

analogues **2a** (para), **4a** (ortho), and **6a** (meta) in CH_2Cl_2 at 298 K. Linkage of one PhC≡C unit to the parent complex [PhC≡CAu(PCy_3)] (**1**) results in red-shifted emission energies. The triplet emission energies of the para (**2a**), ortho (**4a**), and meta (**6a**) complexes are red-shifted from that of **1** by 4335, 3248, and 2361 cm^{-1}, respectively. The red-shifted energies are in the order **2a** > **4a** > **6a**, revealing that the electron is more delocalized in the case of para conjugation than in ortho and meta conjugations, and the $\pi \rightarrow \pi^*$ energy gap order is *p*-PE(2) < *o*-PE(2) < *m*-PE(2). Similar red shifts are observed when one more C≡CAu(PCy_3) arm is added to **1** through para, ortho, and meta ligation (Figure 12, right). The triplet emission energies of **3a** (para), **5a** (ortho), and **7a** (meta) are red-shifted from that of **1** by 3374, 1937, and 983 cm^{-1}, respectively. The contribution of the addition of a C≡CAu(PCy_3) arm to the energy shift is less than that of the addition of a C≡CPh group, as C≡CPh has a longer π-conjugation length than C≡C.

In 2003, Martínez and Bardeen[20a] reported that, progressing through the series of PhC≡CH, 1,3-$(HC\equiv C)_2C_6H_4$, and 1,3,5-$(HC\equiv C)_3C_6H_3$, the low-energy absorption peak has a maximum red shift of 600 cm^{-1} in the absorption spectra, while the high-energy fluorescence peak has a maximum red shift of 2000 cm^{-1} with each additional ethynyl group on the aryl ring. These data revealed that an excitonic coupling interaction is responsible for these unusual red shifts in the fluorescence spectra of *m*-PEs. In the present work, the phosphorescence of all of the meta-conjugated complexes **1**, **7a**, and **8** is switched on through Au−C ligation with $[Au(PCy_3)]^+$ moieties. The difference in the low-energy absorption energies (ΔE_a) is 126 cm^{-1} between **1** and **7a** and is 373 cm^{-1} between **7a** and **8**. The difference in the phosphorescence maxima (ΔE_p) is 983 cm^{-1} between **1** and **7a** and is 462 cm^{-1} between **7a** and **8** (Figure 12, right). The ΔE_p values are generally smaller than those of ΔE_f (the difference between high-energy fluorescence maxima) observed in the naked ligand system (2000 cm^{-1}).[20a] These data support the presence of excitonic coupling interactions between the C≡CAu(PCy_3) arms in the *triplet excited states*, though these coupling interactions are less significant in comparison with the excitonic coupling of corresponding singlet excited states.

In the present study, information on the contribution of meta conjugation (or cross conjugation) to electron delocalization at the triplet excited states could be obtained from both steady-state emission and time-resolved excited-state absorption spectra. With an additional C≡CPh moiety at the meta position, the red shift of the triplet emission maximum from 418 nm for [PhC≡CAu(PCy_3)] (**1**) to 465 nm for [PhC≡CC_6H_4-1,3-C≡CAu(PCy_3)] (**6a**) suggests the presence of an excitonic coupling interaction between the cross-conjugated ethynyl and C≡CPh moieties in the meta configuration. Further extending the repeating unit of the *m*-PEs from **6a** to [PhC≡$C(C_6H_4$-1,3-$C\equiv C)_2$Au(PCy_3)] (**6b**) revealed a minor red shift in the triplet emission maximum from 465 nm for **6a** to 469 nm for **6b**. However, on comparison of the time-resolved excited-state absorption spectra in the picosecond time regime, there is a red shift in the absorption peak maximum from **6a** (at ~425 nm) to **6b** (at ~440 nm), suggesting a slightly larger excited-state electron delocalization for **6b** than for **6a**. The ground-state electron delocalization between two phenylethynyl moieties with a meta configuration (one of the cross conjugations) is virtually blocked. In the excited states, however, excitonic coupling interaction facilitates the electron delocalization between the two *m*-phenylethynyl moieties, which has previously been demonstrated for the singlet excited states by Martínez and Bardeen[20a] in 2003 and for the triplet excited states described in this work.

$\Delta E(S_0-T_1)$ Energies of *o*-PE and *m*-PE Polymers. To examine the relationship between the energies of the lowest triplet excited states T_1 and ligand chain length, the $\Delta E(S_0-T_1)$ (energy gap between S_0 and T_1) is plotted against $1/n$ (n is the number of repeating PE units) (Figure 13). All of the data points of the mononuclear and binuclear complexes of *o*-PE and *m*-PE produce good linearity. Extrapolation of the lines to $1/n = 0$ gives the estimated $\Delta E(S_0-T_1)$ values for the [Au(PCy_3)]-capped complexes containing infinitely repeating PE units. The mononuclear and dinuclear species have the same limiting $\Delta E(S_0-T_1)$ values: for the *p*-PE species, ~600 nm; for the *o*-PE species, ~530 nm; for the *m*-PE species, ~470 nm. This is the first report of the estimated phosphorescence energies of poly(*o*-PE) and poly(*m*-PE), which is useful information for future studies on polymeric PE in ortho and meta analogues.

SUMMARY

In this work, we synthesized mononuclear and binuclear gold(I) complexes containing oligo(*o*-PE or *m*-PE) ligands and examined their photophysical properties. We have performed

detailed spectroscopic studies by using time-resolved fs-TA, fs-TRF, and ns-TRE in conjunction with steady-state absorption and emission methods to directly detect the dynamics, origination, and spectral character of the excited states of these complexes. The complexes were revealed to exhibit ligand-centered dual emission at ambient and low (77 K) temperature with fluorescence from the lowest energy singlet $S_1(^1\pi\pi^*)$ and phosphorescence from $T_1(^3\pi\pi^*)$. Independent of the composition of ligand, ISC from S_1 to T_1 was found to occur on a rapid time scale with nearly unity efficiency. The fluorescence of most the complexes at ambient temperature contains a joint contribution from PF and DF. The PF is observed because of the tens of picoseconds lifetimes of the photoprepared S_1, while the long-lived DF (lifetime on the microsecond time scale) was found to arise due to TTA from T_1. The efficiency of TTA is facilitated by extension of the PE ligand length and is also affected by the substitution pattern of the PE ligand. The ligand-sensitive reactivity of T_1 plays a critical role in dictating the emission behavior of the complexes. The difference in conjugation between *p*-, *o*-, and *m*-PE ligations was studied by comparison of the singlet and triplet emission energies. The triplet emission energies of poly(*o*-PE) and poly(*m*-PE) are estimated to be ~530 and ~470 nm, respectively, by the extrapolation method. Together with the $[Au(PCy_3)]^+$ complexes containing *p*-PE ligands reported previously, all of these complexes constitute a complete class of $[Au(PCy_3)]^+$-supported phenyleneethynylene complexes, which can be used as models for PE-based polymeric/dendritic materials.

EXPERIMENTAL SECTION

General Procedures and Materials. All starting materials were purchased from commercial sources and used as received unless stated otherwise. The solvents used for synthesis were of analytical grade. Details of solvent treatment for photophysical studies have been described earlier.[41] $[(Cy_3P)AuCl]$[42] was prepared according to literature methods. ^1H and ^{13}C NMR spectra were recorded on a Bruker Avance 400 or 300 NMR spectrometer (referenced to residual solvent) at 298 K. ^{31}P NMR spectra were recorded on a Bruker Avance 400 at 298 K. Mass spectra (FAB) were obtained on a Finnigan MAT 95 mass spectrometer. Elemental analyses were performed by the Beijing Institute of Chemistry, Chinese Academy of Sciences. UV−vis spectra were recorded on a Perkin-Elmer Lambda 19 UV/vis spectrophotometer. Emission spectra were obtained on a SPEX Fluorolog-2 fluorescence spectrophotometer. Emission lifetime measurements were performed with a Quanta Ray DCR-3 pulsed Nd:YAG laser system (pulse output 266 nm, 8 ns). Errors for λ values (±1 nm) and τ (±10%) are estimated. The instrumental setups for fs-TRF and fs-TA and the related spectral calibrations have been described previously.[28] Briefly, the fs-TA and fs-TRF as well as ns-TRE measurements were performed with a a commercial Ti:sapphire regenerative amplifier laser system (800 nm, 40 fs, 1 kHz, and 3.5 mJ/pulse). The 280 nm pump pulse was produced from the second harmonic of the sum of the frequency generation between an OPA output and the 800 nm fundamental laser pulse. In fs-TA, the samples were probed by a white light continuum pulse created from a rotating CaF_2 plate pumped by the 800 nm laser. fs-TRF was measured by employing the Kerr-gate technique.[28,43] A Kerr device composed of a 1 mm thickness Kerr medium (benzene contained in a quartz cell) equipped within a crossed polarizer pair was driven by the 800 nm laser to function as an ultrafast optical shutter to sample transient fluorescence spectra at various selected pump/probe delays. For both fs-TA and fs-TRF, the temporal delay of probe to pump pulse was controlled by an optical delay line. The fs-TA or fs-TRF signals were collected by a monochromator and detected with a liquid-nitrogen-cooled CCD detector. The instrument response function (IRF) of fs-TA and fs-TRF is wavelength-dependent. As the detection wavelength varies from 600 to 280 nm, the IRF varies from ~0.5 to ~2 ps for TRF and ~100 to ~300 fs for TA. For the ns-TRE measurements, an intensified CCD (ICCD) detector, which was synchronized to the fs laser system, was used to detect transient emission spectra with the controlled pump/probe time delay covering from ~2 ns and afterward. To eliminate the effect of rotational diffusion, the polarization direction of the pump laser was set at the magic angle in relation to that of probe for all measurements. The measurements were done at room temperature and atmospheric pressure with ~15 mL samples flowed into a cell with 0.5 mm path length. In ns-TRE, the sample solutions were purged with nitrogen gas to diminish the oxygen quenching effect. The samples were monitored by UV−vis absorption and revealed no degradation after the time-resolved measurements.

General Procedure for the Synthesis of Gold(I) Acetylide Complexes. To a mixture of $[(Cy_3P)AuCl]$ (0.11 g, 0.2 mmol for mononuclear species or 0.22 g, 0.4 mmol for binuclear species) and Me_3Si-protected acetylene (0.2 mmol) in dichloromethane/methanol (1/1, 20 mL) was added sodium methoxide (0.04 g). The solution was stirred for 12 h and evaporated to dryness under reduced pressure. The residue was subjected to a short alumina (neutral) plug and eluted with CH_2Cl_2. Recrystallization from dichloromethane/diethyl ether gave a crystalline powder. See the Supporting Information for detailed characterization data.

ASSOCIATED CONTENT

Supporting Information. Text, figures, tables, and a CIF file giving details of synthesis and characterization data for all complexes, crystallographic data for all crystal structures, supplementary photophysical spectra, absorption and emission spectra of the free ligands, and plots of ln k_q' vs $E^\circ(A^+/A)$ for the oxidative quenching of **4a** by pyridinium acceptors in acetonitrile. This material is available free of charge via the Internet at http://pubs.acs.org.

AUTHOR INFORMATION

Corresponding Author
*Email: cmche@hku.hk

ACKNOWLEDGMENT

This work was supported by the University Development Fund of The University of Hong Kong and the Hong Kong Research Grants Council (Nos. HKU 7008/09P and AOE/P-03/08), NSFC/RGC Joint Research Scheme (N-HKU 752/08), and CAS-Croucher Funding Scheme for Joint Laboratories. W.L. thanks The University of Hong Kong for a Research Assistant Professorship.

REFERENCES

(1) (a) Martin, R. E.; Diederich, F. *Angew. Chem., Int. Ed.* **1999**, *38*, 1350–1377.(b) Stang, P. J.; Diederich, F. *Modern Acetylene Chemistry*; VCH: Weinheim, Germany, 1995. (c) Carter, G. M.; Chen, Y. J.; Rubner, M. F.; Sandman, D. J.; Thakur, M. K.; Tripathy, S. K. In *Non-Linear Optical Properties of Organic Molecules and Crystals*; Chemla, D. S., Zyss, J., Eds.; Academic: Orlando, FL, 1987; Vol. 2, Chapter III-3.

(2) (a) Tour, J. M. *Chem. Rev.* **1996**, *96*, 537–554. (b) Schwab, P. F. H.; Levin, M. D.; Michl, J. *Chem. Rev.* **1999**, *99*, 1863–1934. (c) Bunz, U. H. F. *Chem. Rev.* **2000**, *100*, 1605–1644. (d) McQuade, D. T.; Pullen, A. E.; Swager, T. M. *Chem. Rev.* **2000**, *100*, 2537–2574. (e) Hill, D. J.; Mio, M. J.; Prince, R. B.; Hughes, T. S.; Moore, J. S. *Chem. Rev.* **2001**, *101*, 3893–4011.

(3) (a) Grubbs, R. H.; Kratz, D. *Chem. Ber.* **1993**, *126*, 149–157. (b) Baldwin, K. P.; Simons, R. S.; Rose, J.; Zimmerman, P.; Hercules, D. M.; Tessier, C. A.; Youngs, W. J. *J. Chem. Soc., Chem. Commun.* **1994**, 1257–1258. (c) Wong, M. S.; Nicoud, J. F. *Tetrahedron Lett.* **1994**, *35*, 6113–6116. (d) Orita, A.; Yoshioka, N.; Struwe, P.; Braier, A.; Beckmann, A.; Otera, J. *Chem. Eur. J.* **1999**, *5*, 1355–1363. (e) Youngs, W. J.; Tessier, C. A.; Bradshaw, J. D. *Chem. Rev.* **1999**, *99*, 3153–3180. (f) Jones, T. V.; Blatchly, R. A.; Tew, G. N. *Org. Lett.* **2003**, *5*, 3297–3299. (g) Jones, T. V.; Slutsky, M. M.; Laos, R.; de Greef, T. F. A.; Tew, G. N. *J. Am. Chem. Soc.* **2005**, *127*, 17235–17240. (h) Khan, A.; Hecht, S. *J. Polym. Sci., Part A: Polym. Chem.* **2006**, *44*, 1619–1627. (i) Slutsky, M. M.; Phillip, J. S.; Tew, G. N. *New J. Chem.* **2008**, *32*, 670–675. (j) Jones, T. V.; Slutsky, M. M.; Tew, G. N. *New J. Chem.* **2008**, *32*, 676–679.

(4) (a) Devadoss, C.; Bharathi, P.; Moore, J. S. *J. Am. Chem. Soc.* **1996**, *118*, 9635–9644. (b) Tretiak, S.; Chernyak, V.; Mukamel, S. *J. Phys. Chem. B* **1998**, *102*, 3310–3315.

(5) (a) Onitsuka, K.; Yamamoto, S.; Takahashi, S. *Angew. Chem., Int. Ed.* **1999**, *38*, 174–176. (b) MacDonald, M. A.; Puddephatt, R. J. *Organometallics* **2000**, *19*, 2194–2199. (c) Vicente, J.; Chicote, M. T.; Abrisqueta, M. D.; Alvarez-Falcon, M. M. *J. Organomet. Chem.* **2002**, *663*, 40–45. (d) Vicente, J.; Chicote, M. T.; Alvarez-Falcon, M. M.; Abrisqueta, M. D.; Hernandez, F. J.; Jones, P. G. *Inorg. Chim. Acta* **2003**, *347*, 67–74. (e) Zhu, M. X.; Lu, W.; Zhu, N.; Che, C. M. *Chem. Eur. J.* **2008**, *14*, 9736–9746.

(6) (a) Bruce, M. I. *Coord. Chem. Rev.* **1997**, *166*, 91–119. (g) Manna, J.; John, K. D.; Hopkins, M. D. *Adv. Organomet. Chem.* **1995**, *38*, 79–154.

(7) (a) Wohlgenannt, M.; Tandon, K.; Mazumdar, S.; Ramasesha, S.; Vardeny, Z. V. *Nature* **2001**, *409*, 494–497. (b) Wilson, J. S.; Dhoot, A. S.; Seeley, A. J. A. B.; Khan, M. S.; Köhler, A.; Friend, R. H. *Nature* **2001**, *413*, 828–831. (c) Lin, L. C.; Meng, H. F.; Shy, J. T.; Horng, S. F.; Yu, L. S.; Chen, C. H.; Liaw, H. H.; Huang, C. C.; Peng, K. Y.; Chen, S. A. *Phys. Rev. Lett.* **2003**, *90*, 036601. (d) Segal, M.; Baldo, M. A.; Holmes, R. J.; Forrest, S. R.; Soos, Z. G. *Phys. Rev. B* **2003**, *68*, 075211.

(8) (a) Baldo, M. A.; O'Brien, D. F.; You, Y.; Shoustikov, A.; Sibley, S.; Thompson, M. E.; Forrest, S. R. *Nature* **1998**, *395*, 151–154. (b) Wilson, J. S.; Chawdhury, N.; Köhler, A.; Friend, R. H. *Adv. Mater.* **2002**, *14*, 701–707.

(9) Lupton, J. M.; Pogantsch, A.; Piok, T.; List, E. J. W.; Patil, S.; Scherf, U. *Phys. Rev. Lett.* **2002**, *89*, 167401.

(10) (a) Omary, M. A.; Kassab, R. M.; Haneline, M. R.; Elbjeirami, O.; Gabbaï, F. P. *Inorg. Chem.* **2003**, *42*, 2176–2178. (b) Burress, C.; Elbjeirami, O.; Omary, M. A.; Gabbaï, F. P. *J. Am. Chem. Soc.* **2005**, *127*, 12616–12617.

(11) (a) Yuan, W. Z.; Shen, X. Y.; Zhao, H.; Lam, J. W. Y.; Tang, L.; Lu, P.; Wang, C. L.; Liu, Y.; Wang, Z. M.; Zheng, Q.; Sun, J. Z.; Ma, Y. G.; Tang, B. Z. *J. Phys. Chem. C* **2010**, *114*, 6090–6099. (b) Bolton, O.; Lee, K. W.; Kim, H.-J.; Lin, K. Y.; Kim, J. S. *Nature Chem.* **2011**, *3*, 205–210.

(12) (a) Wilson, J. S.; Chawdhury, N.; Köhler, A.; Friend, R. H.; Al-Mandhary, M. R. A.; Khan, M. S.; Younus, M.; Raithby, P. R. *J. Am. Chem. Soc.* **2001**, *123*, 9412–9417. (b) Liu, Y.; Jiang, S.; Glusac, K.; Powell, D. H.; Anderson, D. F.; Schanze, K. S. *J. Am. Chem. Soc.* **2002**, *124*, 12412–12413. (c) Wilson, J. S.; Wilson, R. J.; Friend, R. H.; Köhler, A.; Al-Suti, M. K.; Al-Mandhary, M. R. A.; Khan, M. S. *Phys. Rev. B* **2003**, *67*, 125206.

(13) (a) Che, C. M.; Chao, H. Y.; Miskowski, V. M.; Li, Y.; Cheung, K. K. *J. Am. Chem. Soc.* **2001**, *123*, 4985–4991. (b) Lu, W.; Xiang, H. F.; Zhu, N.; Che, C. M. *Organometallics* **2002**, *21*, 2343–2346. (c) Chao, H. Y.; Lu, W.; Li, Y.; Chan, M. C. W.; Che, C. M.; Cheung, K. K.; Zhu, N. *J. Am. Chem. Soc.* **2002**, *124*, 14696–14706. (d) Lu, W.; Zhu, N.; Che, C. M. *J. Organomet. Chem.* **2003**, *670*, 11–16. (e) Lu, W.; Zhu, N.; Che., C. M. *J. Am. Chem. Soc.* **2003**, *125*, 16081–16088. (f) Tong, G. S. M.; Chow, P. K.; Che., C. M. *Angew. Chem., Int. Ed.* **2010**, *49*, 9206–9209.

(14) Recent examples of spectroscopic studies on Ru(II) complexes: (a) Damrauer, N. H.; Cerullo, G.; Yeh, A.; Boussie, T. R.; Shank, C. V.; McCusker, J. K. *Science* **1997**, *275*, 54–57. (b) Yeh, A.; Shank, C. V.; McCusker, J. K. *Science* **2000**, *289*, 935–938. (c) Bhasikuttan, A. C.; Suzuki, M.; Nakashima, S.; Okada, T. *J. Am. Chem. Soc.* **2002**, *124*, 8398–8405. (d) Browne, W. R.; Coates, C. G.; Brady, C.; Matousek, P.; Towrie, M.; Botchway, S. W.; Parker, A. W.; Vos, J. G.; McGarvey, J. J. *J. Am. Chem. Soc.* **2003**, *125*, 1706–1707. (e) Cannizzo, A.; Mourik, F.; Gawelda, W.; Zgrablic, G.; Bressler, C.; Chergui, M. *Angew. Chem., Int. Ed.* **2006**, *45*, 3174–3176.

(15) Recent examples of spectroscopic studies on Re(I) complexes: (a) Cannizzo, A.; Blanco-Rodrguez, A. M.; Nahhas, A. E.; Šebera, J.; Záliš, S.; Vlček, A.; Chergui, M. *J. Am. Chem. Soc.* **2008**, *130*, 8967–8974. (b) Nahhas, A. E.; Cannizzo, A.; Mourik, F.; Blanco-Rodríguez, A. M.; Záliš, S.; Vlček, A.; Chergui, M. *J. Phys. Chem. A* **2010**, *114*, 6361–6369. (c) Busby, M.; Matousek, P.; Towrie, M.; Vlček, A. *J. Phys. Chem. A* **2005**, *109*, 3000–3008. (d) Liard, D. J.; Busby, M.; Farrell, I. R.; Matousek, P.; Towrie, M.; Vlček, A. *J. Phys. Chem. A* **2004**, *108*, 556–567.

(16) Recent examples of spectroscopic studies on Pt(II) complexes: (a) Ramakrishna, G.; Goodson, T., III; Rogers-Haley, J. E.; Cooper, T. M.; McLean, D. G.; Urbas, A. *J. Phys. Chem. C* **2009**, *113*, 1060–1066. (b) Abedin-Siddique, Z.; Ohno, T.; Nozaki, K.; Tsubomura, T. *Inorg. Chem.* **2004**, *43*, 663–673. (c) Whittle, C.; Weinstein, J. A.; George, M. W.; Schanze, K. S. *Inorg. Chem.* **2001**, *40*, 4053–4062. (d) Hissler, M.; Connick, W. B.; Geiger, D. K.; McGarrah, J. E.; Lipa, D.; Lachicotte, R. J.; Eisenberg, R. *Inorg. Chem.* **2000**, *39*, 447–457.

(17) Gawelda, W.; Cannizzo, A.; Pham, V.-T.; Mourik, F.; Bressler, C.; Chergui, M. *J. Am. Chem. Soc.* **2007**, *129*, 8199–8206.

(18) Recent examples of spectroscopic studies on Ir(III) complexes: (a) Quochi, F.; Saba, M.; Artizzu, F.; Mercuri, M. L.; Deplano, P.; Mura, A.; Bongiovanni, G. *J. Phys. Chem. Lett.* **2010**, *1*, 2733–2737. (b) Ramachandra, S.; Polo, F.; Edafe, F.; Schuermann, K. C.; Nijhuis, C. A.; Belser, P.; Reus, W. F.; Whitesides, G. M.; De Cola, L. *Pure Appl. Chem.* **2011**, *83*, 779–799.

(19) Steffen, A.; Tay, M. G.; Batsanov, A. S.; Howard, J. A. K.; Beeby, A.; Vuong, K. Q.; Sun, X.-Z.; George, M. W.; Marder, T. B. *Angew. Chem., Int. Ed.* **2010**, *49*, 2349–2353.

(20) (a) Gaab, K. M.; Thompson, A. L.; Xu, J. J.; Martínez, T. J.; Bardeen, C. J. *J. Am. Chem. Soc.* **2003**, *125*, 9288–9299. (b) Thompson, A. L.; Gaab, K. M.; Xu, J.; Bardeen, C. J.; Martínez, T. J. *J. Phys. Chem. A* **2004**, *108*, 671–682.

(21) Yam, V. W. W.; Tao, C. H.; Zhang, L. J.; Wong, K. M. C.; Cheung, K. K. *Organometallics* **2001**, *20*, 453–459.

(22) Devadoss, C.; Bharathi, P.; Moore, J. S. *J. Am. Chem. Soc.* **1996**, *118*, 9635–9644.

(23) Anderson, S. *Chem. Eur. J.* **2001**, *7*, 4706–4714.

(24) (a) Bruce, M. I.; Horn, E.; Matisons, J. G.; Snow, M. R. *Aust. J. Chem.* **1984**, *37*, 1163–1170. (b) Cross, R. J.; Davidson, M. F. *J. Chem. Soc., Dalton Trans.* **1986**, 411–414. (c) Jia, G.; Puddephatt, R. J.; Scott, J. D.; Vittal, J. J. *Organometallics* **1993**, *12*, 3565–3574. (d) Naulty, R. H.; Cifuentes, M. P.; Humphrey, M. G.; Houbrechts, S.; Boutton, C.; Persoons, A.; Heath, G. A.; Hockless, D. C. R.; Luther-Davies, B.; Samoc, M. *J. Chem. Soc., Dalton Trans.* **1997**, 4167–4174.

(25) Li, D.; Hong, X.; Che, C. M.; Lo, W. C.; Peng, S. M. *J. Chem. Soc., Dalton Trans.* **1993**, 2929–2932.

(26) Yam, V. W. W.; Choi, S. W. K. *J. Chem. Soc., Dalton Trans.* **1996** 4227–4232.

(27) (a) Duvanel, G.; Grilj, J.; Schuwey, A.; Gossauer, A.; Vauthey, E. *Photochem. Photobiol. Sci.* **2007**, *6*, 956–963. (b) Liu, L. T.; Yaron, D. J.; Sluch, M. I.; Berg, M. A. *J. Phys. Chem. B* **2006**, *110*, 18844–18852.

(28) (a) Kwok, W. M.; Ma, C.; Phillips, D. L. *J. Am. Chem. Soc.* **2006**, *128*, 11894–11905. (b) Kwok, W. M.; Ma, C.; Phillips, D. L. *J. Am. Chem. Soc.* **2008**, *130*, 5131–5139.

(29) Turro, N. J. *Modern Molecular Photochemistry*; University Science Books: Mill Valley, CA, 1991.

(30) (a) Liard, D. J.; Busby, M.; Matousek, P.; Towrie, M.; Vlček, A. *J. Phys. Chem. A* **2004**, *108*, 2363–2369. (b) Hester, R. E.; Matousek, P.; Moore, J. N.; Parker, A. W.; Toner, W. T.; Towrie, M. *Chem. Phys. Lett.* **1993**, *208*, 471–478. (c) Matousek, P.; Parker, A. W.; Towrie, M.; Toner, W. T. *J. Chem. Phys.* **1997**, *107*, 9807–9817. (d) Weaver, W. L.; Huston, L. A.; Iwata, K.; Gustafson, T. L. *J. Phys. Chem.* **1992**,

96, 8956–8961. (e) Iwata, K.; Hamaguchi, H. *J. Phys. Chem. A* **1997**, *101*, 632–637.
(31) Sluch, M. I.; Godt, A.; Bunz, U. H. F.; Berg., M. A. *J. Am. Chem. Soc.* **2001**, *123*, 6447–6448.
(32) (a) Swenberg, C. E. *J. Chem. Phys.* **1969**, *51*, 1753–1764. (b) Azumi, T.; McGlynn, S. P. *J. Chem. Phys.* **1963**, *39*, 1186–1194.
(33) Bohne, C.; Abuin, E. B.; Scaiano, J. C. *J. Am. Chem. Soc.* **1990**, *112*, 4226–4231.
(34) Turek, A. M.; Krishnamoorthy, G.; Phipps, K.; Saltiel, J. *J. Phys. Chem. A* **2002**, *106*, 6044–6052.
(35) (a) Gerhard, A.; Bässler, H. *J. Chem. Phys.* **2002**, *117*, 7350–7356. (b) Hertel, D.; Bässler, H. *J. Chem. Phys.* **2001**, *115*, 10007–10013. (c) Hertel, D.; Setayesh, S.; Nothofer, H.-G.; Scherf, U.; Müllen, K.; Bässler, H. *Adv. Mater.* **2001**, *13*, 65–69. (d) Romanovskii, Y. V.; Bässler, H. *Chem. Phys. Lett.* **2000**, *326*, 51–57.
(36) Bodunov, E. N.; Berberan-Santos, M. N.; Martinho, J. M. G. *Chem. Phys.* **2005**, *316*, 217–224.
(37) (a) Partee, J.; Frankevich, E. L.; Uhlhorn, B.; Shinar, J.; Ding, Y.; Barton, T. J. *Phys. Rev. Lett.* **1999**, *82*, 3673–3676. (b) Baldo, M. A.; Adachi, C.; Forrest, S. R. *Phys. Rev. B* **2000**, *62*, 10967–10977. (c) Baldo, M. A.; Forrest, S. R. *Phys. Rev. B* **2000**, *62*, 10958–10966.
(38) Abedin-Siddique, Z.; Yamamoto, Y.; Ohno, T.; Nozaki, K. *Inorg. Chem.* **2003**, *42*, 6366–6378.
(39) Marshall, J. L.; Stobart, S. R.; Gray, H. B. *J. Am. Chem. Soc.* **1984**, *106*, 3027–3029.
(40) Jones, R. R.; Bergman, R. G. *J. Am. Chem. Soc.* **1972**, *94*, 660–661.
(41) Chan, S. C.; Chan, M. C. W.; Che, C. M.; Wang, Y.; Cheung, K. K.; Zhu, N. *Chem. Eur. J.* **2001**, *7*, 4180–4190.
(42) Al-sa'ady, A. K.; McAuliffe, C. A.; Parish, R. V.; Sandbank, J. A. *Inorg. Synth.* **1985**, *23*, 191–194.
(43) (a) Matousek, P.; Towrie, M.; Ma, C.; Kwok, W. M.; Phillips, D.; Toner, W. T.; Parker, A. W. *J. Raman Spectrosc.* **2001**, *32*, 983–988. (b) Matousek, P.; Towrie, M.; Stanley, A.; Parker, A. W. *Appl. Spectrosc.* **1999**, *53*, 1485–1489.